Design and Fabrication of a 3D Printed Compact LC Sensor

by

Amirhossein Hassanpoor Kalhori

B.Sc., University of Tehran, 2019

Thesis Submitted in Partial Fulfillment of the
Requirements for the Degree of
Master of Applied Science

in the
School of Mechatronic Systems Engineering
Faculty of Applied Sciences

SIMON FRASER UNIVERSITY
Fall 2022

Declaration of Committee

Name:	**Amirhossein Hassanpoor Kalhori**
Degree:	**Master of Applied Science**
Thesis title:	**Design and Fabrication of a 3D Printed Compact LC Sensor**
Committee:	**Chair: Ahad Armin** Lecturer, Mechatronic Systems Engineering
	Woo Soo Kim Supervisor Professor, Mechatronic Systems Engineering
	Jiacheng (Jason) Wang Committee Member Associate Professor, Mechatronic Systems Engineering
	Vincenzo Pecunia Examiner Associate Professor, Sustainable Energy Engineering

Abstract

Robotics, wearable technology, and prosthetics are all advancing thanks to the development of wireless sensing technologies. The ability of wireless passive radio frequency (RF) devices, such as LC (inductor-capacitor) resonators, to operate in a variety of sensing areas such as pressure, temperature, and location identification without the need for power supplies has made them stand out among other types of sensing devices. However, passive LC sensors suffer from short-range wireless detection, and their fabrication process requires several stages. Here, we propose a new design of compact LC-based wireless location identification sensors fabricated by the direct ink writing (DIW) 3D printing method. Furthermore, a wireless sensing system has been proposed which consists of LC sensors and RF communication that increases the wireless reading distance to about ten centimeters. Finally, a dielectric material with high dielectric permittivity has been employed to amplify the quality factor of the wireless sensors.

Keywords: RF Sensing; LC Resonator; 3D printed sensor; Dielectric Materials; Wireless sensor

Dedication

To my brave people in Iran, who are risking their lives fighting against the dictatorship.

Acknowledgments

First and foremost, I would like to acknowledge my senior supervisor Dr. Woo Soo Kim without which none of this would be possible. I have learned much about setting goals, planning to achieve them, and being consistent. For that I am grateful. Above all, I am thankful for his patience and guidance throughout this long journey, and his words of encouragement in challenges during these two years. A tremendous thanks to him for his supervision.

I would like to further appreciate my supervisory committee, Dr. Jason Wang, for his valuable feedback and suggestions on my research project. Moreover, I would like to thank Dr. Vincenzo Pecuina and Dr. Ahad Armin for their time and consideration.

Furthermore, I would like to thank my lovely wife, Sogol, whose pure support has been my encouragement. Thank you for trusting me and being by my side through this journey we began.

To the new friends I have made in the Additive Manufacturing Lab, I would like to thank you for your continued support throughout this process. Thank you, Tae-Ho, Wonchul, Haotian, Hadi, and Chao, for always being able to help me with my project. Moreover, I would like to thank the colleague and friend we lost this year. Thank you Seapehi for being supportive and helpful. Moreover, I would like to thank the National Research Council of Canada (NRC)'s 3D printing team for giving me the opportunity to collaborate and for their valuable feedback.

Lastly, I would like to extend my utmost gratitude to my family (Father, Mother, and Brother) who encouraged me to study, find my passion, and help me become a better man. Your support led me to the position I am in right now. You always have a special place in my heart.

Table of Contents

List of Tables

List of Figures

List of Acronyms

AFN	Aerodynamically Focused Nanomaterial
AgNW	Silver Nanowire
CAD	Computer Assisted Design
CNC	Cellulose Nanocrystals
CNF	Cellulose Nanofibers
CNT	Carbon Nanotube
DIW	Direct-ink Writing
FDM	Fused Deposition Modeling
FEA	Finite Element Analysis
IC	Integrated Circuit
IDC	Interdigitated Capacitor
IDE	Interdigitated Electrode
IoT	Internet of Things
ISME	Ion-selective Membrane Electrode
MWCNT	Multi-wall Carbon Nanotubes
NFC	Near-field Communication
PDMS	Polydimethylsiloxane
PET	Polyethylene Terephthalate
PMMA	Polymethyl Methacrylate
PTC	Positive Temperature Coefficient
SLS	Selective Laser Sintering
SMA	Sub Miniature version A
SRR	Split Ring Resonator
RF	Radio Frequency
RFID	Radio Frequency Identification
VNA	Vector Network Analyzer
VOC	Volatile Organic Compounds

Author's Contributions

This thesis reports the original research works conducted during the period of my Master of Applied Science degree in the school of mechatronic systems engineering at Simon Fraser University. Parts of this thesis include the introduction and results discussed in the journal manuscripts submitted for "*Flexible and Printed Electronics – IOPScience*" and accepted for "*ACS Applied Electronic Materials*" in 2022.

Executive Summary

As the world shifts towards the IoT era, wireless sensors present themself as an essential technology in the transition. Radio frequency wireless sensors have been attractive in this matter because of the numerous merits that they can provide such as the ability of wireless sensing without the need of complex circuits and power supplies. However, there are some challenges for these sensors such as the limited distance between them and the reader antenna and their fabrication requires several steps and is not cost-effective in terms of time and materials. On the other hand, printing technologies especially conductive 3D printing have received tremendous attention in recent years. Benefits of 3D printed electronics include low-cost manufacturing with high efficiency, compatibility with different systems, and relatively easy operation. Here, we propose a wireless radio frequency sensing system with newly designed compact LC sensors, 3D printed by direct ink writing method in a single fabrication step which allows far-field wireless communication as shown in Figure 1.

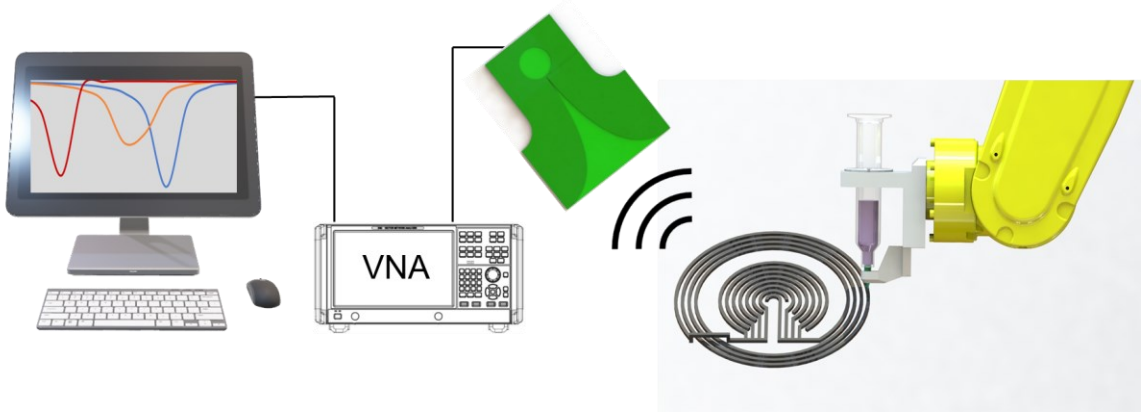

Illustration of 3D printed wireless LC sensor.

Chapter 1. Introduction

1.1. Motivation & Objectives

Advances in sensing technologies pave the way for the internet of the things (IoT) and the 4th industrial revolution. Usual sensor devices require wired data transmission, complex integrated circuits (IC) for wireless communication, and power resources. Efforts to improve the sensing technologies in terms of accuracy, sustainability, and wireless communication between sensors and receiver is ongoing. In the past decade radio frequency (RF) sensors have been a focused study for many researchers because of their advantages such as simple operation and wireless communication without the need for complex chips or power supply. In a meantime, LC sensors are a simple type of RF sensor consisting of an inductor and a capacitor in resonance, which have the potential to sense parameters such as pressure, strain, temperature, and ion wirelessly and without the need for a power source. However, LC sensors suffer from short readout distance which is the distance between them and the reader antenna in wireless communications. Another challenge is the fabrication of LC sensors which requires several steps which can be inefficient and uneconomical.

In this thesis project, we are motivated to overcome those mentioned challenges of conventional LC wireless sensors. We design compact LC sensors and integrate them with radio frequency identification techniques to develop a reliable wireless sensing system with an improved detection range for location identification sensing applications. Furthermore, the cost-efficient fabrication of sensors and RF antenna tags is demonstrated by the direct ink writing (DIW) 3D printing method.

The objective of this thesis project is to design compact and 3D printable LC sensors, by using the DIW 3D printing technique to fabricate designed LC sensors with conductive ink in a single step, introducing an RF sensing tag consisting of LC sensor to achieve the far-field wireless communication, and finally, preparing and utilizing a high permittivity material to improve the wireless communication of the 3D printed RF sensors.

1.2. Thesis Overview

The thesis has been divided into five chapters. In chapter 1, concepts related to the research topic are discussed and reviewed. The discussion begins with an overview of radio frequency sensing systems, consisting of a summary of wireless LC sensor and its mechanism, and radio frequency identification tags. Finally, a spotlight on printed wireless radio frequency sensors in different physical and chemical application are discussed in the chapter. Chapter 2 discusses conventional methods of LC sensor design and the proposed design and fabrication of compact LC sensors. Chapter 3 highlights the finite element analysis of LC sensors. Chapter 4 discusses the experimental analysis and results of wireless radio frequency sensors. Finally, chapter 5 summarizes the outcomes and suggests future works.

1.3. Radio Frequency Sensing Systems

One of the most crucial elements of the next industrial revolution is sensing technology [1]. Sensors are devices that detect and respond to changes in an environment [2]. There are numerous applications of sensing devices such as physical sensing (pressure [3], strain [4], and temperature [5]) and chemical sensing (environmental [6] and bio-medical [7]). Usual sensors typically require a wired terminal connection for transmitting data or work wirelessly using a Bluetooth module or a complex integrated circuit (IC) which requires an extra complex circuit board and power supply [8]. Recently, radio frequency (RF) sensors and radio frequency identification (RFID) have emerged with benefits such as wireless communication, simple operation, and vast application [9]. RF tags contain integrated circuits called an integrator, and an antenna, which are used to transmit data to an RF reader, then the reader converts the radio waves to a more usable form of data [10], [11]. Therefore, each RF tag has a signature frequency called resonant frequency, and based on the sensing applications, any changes in the input can alter the resonant frequency, so by reading the difference in the resonant frequency, the change of the input can be monitored and analyzed [12], [13].

1.3.1. Wireless LC Sensors

A wireless LC sensor is a type of RF sensor which has a capacitor (C) in resonance with an inductor (L). Usually, the capacitor changes in response to the parameter of interest, and the resonant frequency changes with external effects. To wirelessly interrogate the *LC* sensor, a readout coil is magnetically coupled with the sensor, and the resonant frequency of the sensor is detected by monitoring the impedance or input return loss of the readout coil [14]. Therefore, LC sensors can work wirelessly without the need for a battery or any kind of power source [15]. The resonant frequency of the series LC circuit with an inductance of L_S and a capacitance of C_S can be expressed as equation 1.1 and the quality factor of the LC circuit with a total resistance of R_S can be calculated from equation 1.2 [14].

$$f = \frac{1}{2\pi\sqrt{C_S L_S}} \tag{1.1}$$

$$Q = \frac{1}{R_S}\sqrt{\frac{L_S}{C_S}} \tag{1.2}$$

The resonant frequency of the sensor can be obtained via electromagnetic coupling between the readout coil and the inductor of the LC sensor. For one port measurement system with the coil antenna, the input return loss (S11) parameter or reflection coefficient is measured in the desired frequency range. The frequency in which S11 is the minimum is close to the resonant frequency, therefore with this method resonant frequency of the LC sensor can be measured [15].

LC sensors have been widely used for the detection of changes in pressure [16], temperature [17], humidity [18], and chemical [19] wirelessly. Continuous wireless monitoring without the need for a power supply, cost-effectiveness, and long service life are the main advantages of wireless LC sensors [14]. These merits make wireless LC sensors useful in cases where wired connections are difficult, like sealed environments [20], biomedical implants [21], and IoT fields.

An example of the pressure LC sensor and its operation is shown in figure 1.1. In this work, Sun et al. [22] introduced a flexible wireless passive LC pressure sensor that can be attached to different body parts for the measurement of human body motions by

measuring the pressure. When the state of limb motion changes, the resonance frequency of the flexible LC pressure sensor changes. A readout coil connected to the vector network analyzer (VNA) is used to wirelessly interrogate the resonance frequency of the sensor. The VNA can transmit a series of sweep signals which contain the resonance frequency of the sensor to the readout coil, which is magnetically coupled with the inductor of the LC sensor. When the frequency of the electromagnetic signal in the readout device corresponds to the resonance frequency of the sensor, electromagnetic energy was maximally absorbed by the sensor. Therefore, the S11 of the readout device at this resonance frequency reaches the minimum [23]. By analyzing the resonance frequency shift of the sensor, the different motion states of the body part can be analyzed.

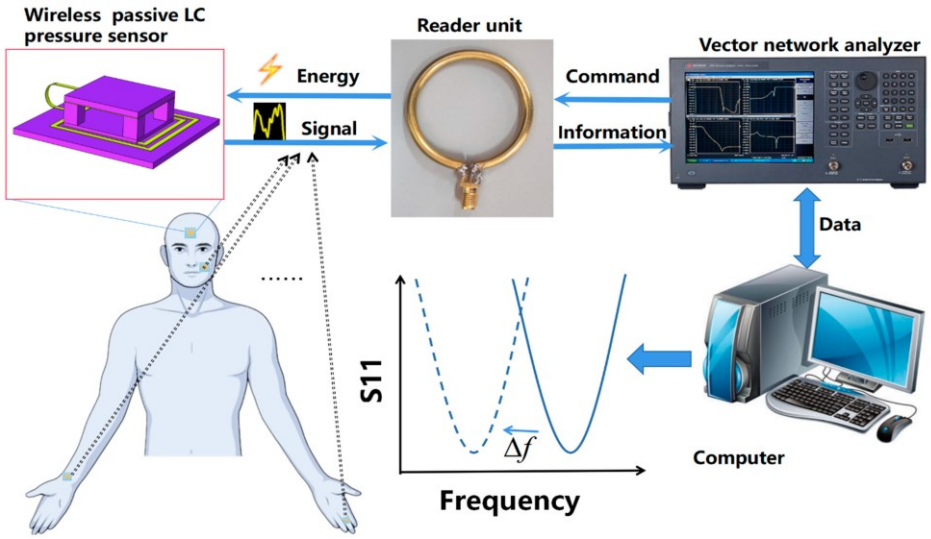

Figure 1.1. Illustration of working operation of an LC pressure sensor for body motion detection. Reprinted with permission [22], Copyright © 2021, micromechanics.

One major challenge of using LC sensors is that they suffer from limited readout distance known as working distance, (less than 1 cm) because of the dispersion of the electromagnetic fields, and the weak magnetic coupling between the sensor and the readout antenna, as the principle of LC sensors is based on electromagnetic coupling [24].

In recent years, many researchers have worked on improving the performance of the LC sensors for sensitivity, detection range, and response time [25]. Some developments such as using an adaptive repeater [24] or dual-inductance resonator [26] have been proposed

to increase the short reading distance up to four cm, but they couldn't exceed this low detection range.

1.3.2. Radio Frequency Identification

Radio frequency identification (RFID) is a wireless data-capturing technique, which utilizes radio frequency (RF) waves for the automatic identification of objects. RFID relies on RF waves for data transmission between the data-carrying device called the RFID transponder and the interrogator [27], [28]. There are two types of RFID tags which are passive and active. A passive type of RFID tag does not require a complex chip or power supply for an operation which makes it cost-efficient [29]. Far-field wireless communication, low fabrication cost, and simple working operation make passive RFID a strong candidate for long-range wireless communication [30].

Figure 1.2 shows an illustration of a chip-less RFID tag and its wireless communication procedure. A passive or chip-less tag is comprised of multiple resonant elements (resonators) that generate a distinct frequency signature. The tag encodes data by using a multi-resonator. The multi-resonator consists of cascaded microwave spiral resonators coupled to a microstrip transmission line. The microwave spiral resonators must be fully planar, exhibit narrow bandwidth meaning a high Q factor, and be compact in size for use in the printable chip-less tag. Resonators can have different geometrical shapes with various electromagnetic behaviors that directly affect the electromagnetic energy absorption, and the resonant frequency. Moreover, an RFID tag comprises a reader antenna to receive the ultra-wideband interrogation signal from the RFID reader (VNA), and a transmitter to send back the encoded signal to the VNA. The VNA also has two antennas for sending and receiving data. In these types of wireless communications of RFID tags with two antennas, the transmission coefficient (S21) is measured in the desired frequency range. Similar to the S11 measurement which was discussed in 1.3.1 the frequency in which S21 is the minimum is close to the resonant frequency of the resonator of the RFID tag [31], [32].

Because of the aforementioned benefits and simple operation, recently, researchers started to use passive RFID tags for different sensing applications which will be discussed in what follows.

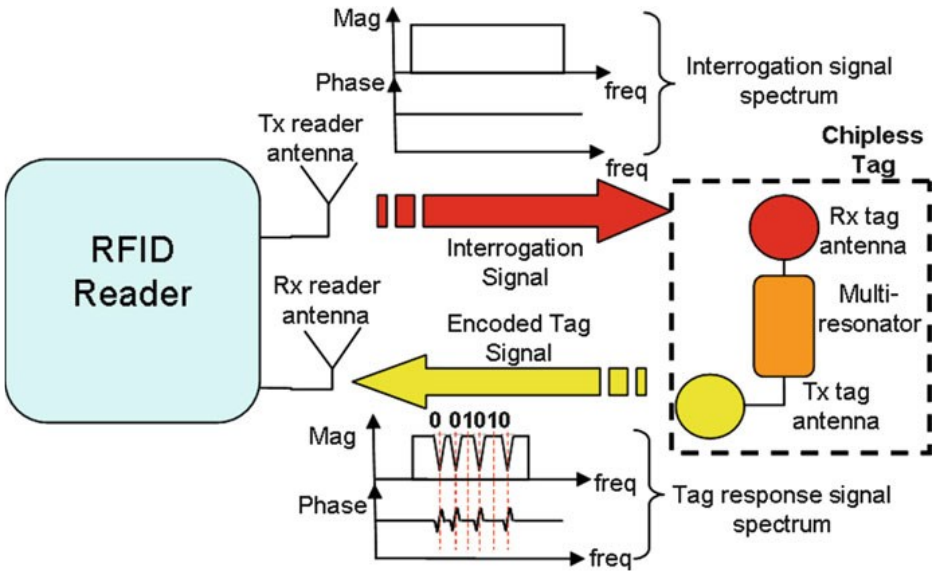

Figure 1.2. Principal diagram of a chip-less RFID system. Reprinted with permission [31], Copyright © 2012, Springer Nature.

1.4. Printing Methods of Electronics

There are different printing methods including screen printing [33], flexography [34], and offset lithography [35] for the fabrication of printed circuits. In the past decade, various 3D printing technologies have been developed for the fabrication of electronic circuits [36]. For example, fused deposition modeling (FDM) has mserits such as high printing speed and low setup cost, but its low resolution, frequent nozzle clogging, and process instability make it challenging for conductive printing [37], [38]. Ink Jet printing has been spotlighted as a representative printing method that despite the fact it is suitable for various substrates and produces fewer wastes, is limited to a planar surface and has nozzle clogging issues [39], [40].

Direct ink writing (DIW)-based 3D printing has recently emerged as an appealing fabrication method of electronic circuits in which a nozzle moves in the desired pattern and deposits conductive ink [41], [42]. This method allows to print of conductive complex patterns in different layers with excellent mechanical properties, and without wasting any

material [43], [44]. Because of the aforementioned benefits, DIW 3D printing method has been used recently for the fabrication of electronic devices and LC sensors [19], [45]-[47].

In printing technologies for RF devices, some of the critical elements are conductive structures, interconnects, and contacts. So, one of the most important parameters is the conductivity of printed materials which has to be high enough [48], [49]. Different printable conductive nanomaterials, such as metal nanomaterials (e.g., metal nanoparticles and metal nanowires) and carbon nanomaterials (e.g., graphene and carbon nanotubes (CNTs)), have been investigated and used as major conductive materials for printed electronics for RF sensors and RFID tags [50]-[53]. To use conductive nanomaterials for printing and deposition, a specific formulation of suitable inks is required [42], [54]. After the deposition of inks on different substrates, post-printing treatment is required to obtain highly conductive patterns which usually is thermal sintering [42]. Alternatively, for being more compatible with common flexible and elastic substrates, different post-printing treatment methods are required to avoid degradation of the substrate, reduce the manufacturing costs, and shorten the processing time such as selective laser sintering (SLS), or microwave sintering [55], [56]. Table 1 compares different conductive materials for printing electronics.

As an example, to create three-dimensional (3D) integration of RF devices, the 3D printing technology such as Direct Ink Writing (DIW) has been demonstrated for the preparation of an inductance-capacitance (LC) RF sensor using a silver nanoparticle ink like figure 1.3. By applying air pressure to the syringe, the conductive ink is dispensed from the nozzle to the substrate. A robot arm moves alongside the desired pattern to print the conductive path to integrate multiple layers for 3D integration.

Table 1.1. Conductive printing materials and their printing methods.

Conductive Materials	Printing Methods	Conductivity (S/m)	Sintering/Curing Method
Carbon Nanotube	Ink-jet Screen printing	$5x10^3$	none
Silver Nanoparticles	Ink-jet Screen Printing DIW	$3.45x10^7$	110°C / 30 min
Silver Nanowires	Screen Printing Ink-jet DIW	$6.3x10^9$	Laser
Liquid Metal (eGaIn)	3D Printing Deposition	$3.9x10^6$	none

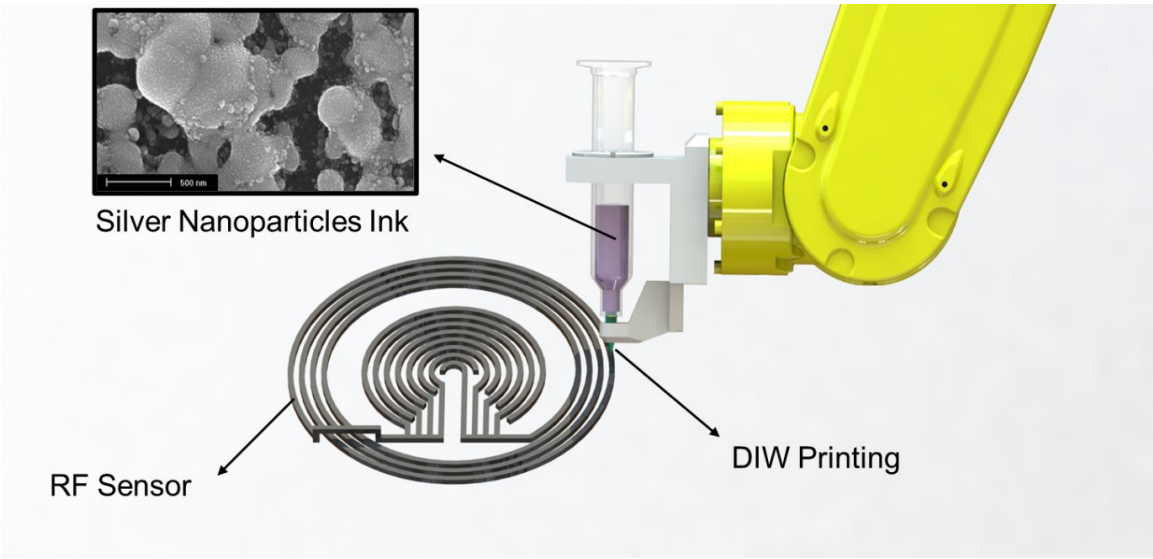

Figure 1.3. Schematic of 3D printing of a compact RF sensor with a silver nanoparticle ink.

1.5. Wireless RF Sensing Applications with the Printed Conductive Materials

In this part, we will overview the recent advances in RF sensing technologies which are printed by conductive materials such as metal nanomaterial-based printable inks and carbon nanomaterial-based printable inks in the fields of physical sensing for pressure, strain, and temperature, and chemical sensing for environmental and biomedical sensing methods.

1.5.1. Pressure Sensing

One of the most widely used physical sensing techniques is pressure sensing, which has applications in the biomedical, automotive, aerospace, and robotics industries, such as posture recognition, monitoring pressurization in aircraft and space habitats, and measuring tank pressurization, etc. [57], [58]. In recent years wireless RF-based pressure sensors have been studied widely. Sensing mechanisms for pressure sensing designs are included, but not limited to resistive or capacitive measurement. By applying pressure to the sensor, the change in resistance or capacitance can be measured wirelessly. Therefore, by experimental methods, the applied pressure causes changes in resistance or capacitance, and it can be monitored and used in the desired applications [12], [59], [60].

Khuje et al. [61] reported the wireless dynamic pressure sensor using flexible copper nanowires, which works by resistance changes. Figure 1.4.a shows the schematic process of copper-based nanowire materials, flexible substrates, and fabrication of their pressure sensor. As shown in figure 1.4.a, two different types of copper nanowires have been used for the fabrication of their sensor. First, sensors fabricated with bare copper nanowires are characterized under ambient conditions. Second, copper nanowires with graphene coatings have been used for severe environment sensing. Mechanically flexible copper nanowires have been selected to construct the resistive sensing network by precisely controlling the nanostructuring of the material, which makes the fine-tuning of the sensitivity. An extrusion-based printer using high-throughput direct writing is selected for the manufacturing of sensors. Since the printed pattern requires to hold its shape and prevent an unwanted flow on the substrate, the rheological properties of the ink play an important role during printing. Moreover, it is also suitable for printing at different speeds,

which permits a high throughput. This printing technique is advantageous because of the easy fabrication of the sensors in larger quantities and being economical. The sensor circuit consists of four-line patterns sandwiched together orthogonally. The sensitivity of the flexible sensor depends on the contact area variation resulting in a change in the contact resistance of the intertwined nanowire structural materials. When the pressure is applied, the printed copper nanowires deform, and the contact area between the adjacent nanowire geometries increases. Then this leads to a decrease in resistance, which can be monitored electrically in a resonant circuit by changing the intensity of the resonant frequency of the circuit, which can be recorded wirelessly [62].

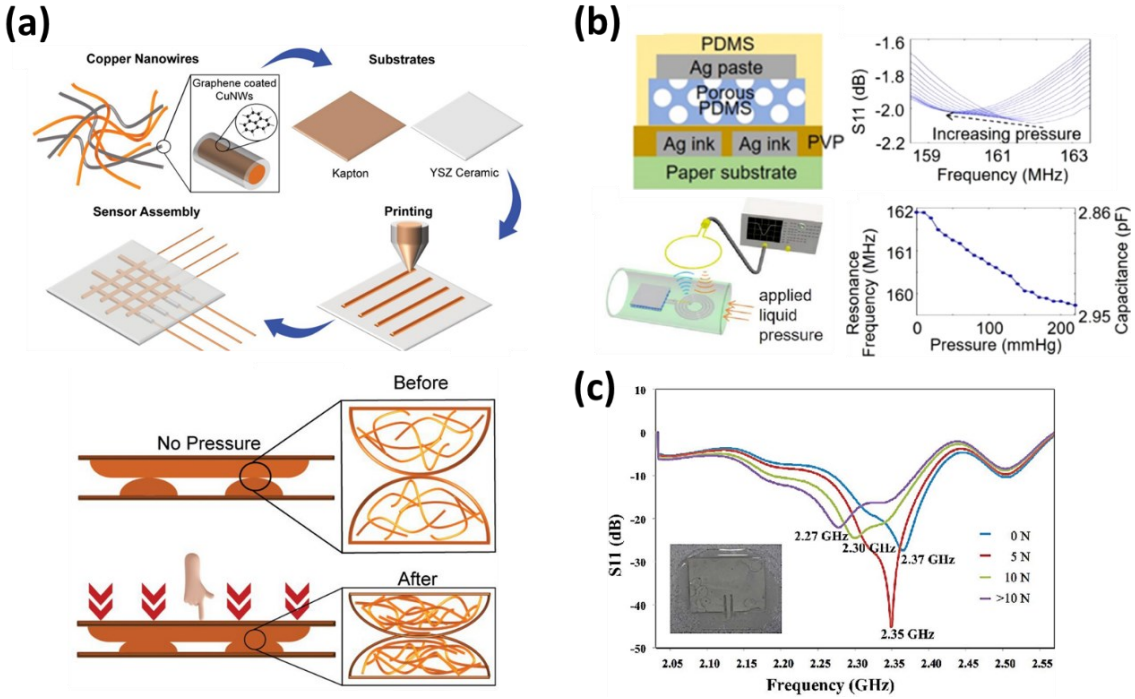

Figure 1.4. **RF pressure sensing. (a) Illustration of sensor fabrication with the copper-based nanowires, and effect of pressure on the structure of printed traces. Reproduced with permission from ref. [61]. Copyright © 2018, American Chemical Society. (b) Schematic of the LC pressure sensor, sensing operation and results. Reproduced with permission from ref. [63]. Copywrite © 2021, IOP Publishing. (c) Results from RFID Pressure tag. Reprinted with permission from ref. [64]. Copyright © 2013, IEEE.**

In another study by Zhai et al. [63] a printed wireless RF fluidic pressure sensor has been proposed which functions by monitoring the pressure in an aqueous environment. As shown in figure 1.4.b, a flexible porous elastomer has been used as a dielectric between the capacitor electrodes in the design and fabrication of the sandwich structure LC sensor. The elastomer polydimethylsiloxane (PDMS) solution is mixed with sacrificial polymethyl methacrylate (PMMA) microspheres. After annealing, the film is submerged in dichlorobenzene that dissolves away the PMMA microspheres to leave behind pores in the dielectric. To fabricate the top stretchable electrode, PDMS was diluted with hexane in a 1:2 ratio by weight and spin-coated on a glass substrate as a buffer layer. The PDMS buffer layer was cured at 120 °C for 10 min. PDMS was mixed with silver paste (Ag/ AgCl ink) in a 1:7 weight ratio, and the mixture was blade coated onto the buffer layer of PDMS. The sample was cured at 120 °C for 30 min to form an Ag electrode. Nanoparticle silver ink has been inkjet printed on a paper substrate and thermally sintered to form the bottom electrode and spiral inductor. As shown in figure 1.4.b, by using a VNA and a coil antenna, the LC sensor can wirelessly communicate, and the resonant frequency of the LC sensor can be monitored. After applying a liquid pressure, the porous dielectric will be compressed and the distance between the two electrodes of the capacitor will be decreased, which leads to a capacitance increase. By increasing the capacitance, the resonant frequency of the LC sensor decreases, so by reading the resonant frequency variation, the change in the applied pressure will be found, as it has been demonstrated in the graphs in figure 1.4.b.

Rai et al. [64] reported a flexible and stretchable RFID patch antenna that can sense the force up to higher than 10 N. They embedded silver nanowires (AgNW) onto the surface of PDMS. Figure 1.4.c shows the fabricated RFID antenna and its resonant frequency changes by applying force on it. In another study, Nikbakhtnasrabadi et al. [65] printed an LC resonator tank with Ag paste to utilize in a wireless smart pressure sensor bandage which can be used in bio-medical applications by screen-printing. There are other studies in printed RF pressure sensors employing conductive materials with various sensing and fabrication methods that pave the way for future advances in wireless RF pressure sensing in many applications.

1.5.2. Strain Sensing

In the past few decades, stretchable electronics have been demonstrated in several engineering fields including wearable or skin-mountable devices, soft robotics, and human-machine interfaces [66], [67]. One of the key elements of stretchable electronics has been strain sensors, which have several applications including acoustic measurement, human-motion monitoring, and structural health monitoring [68]-[70]. Recently, RF technology is widely used for wireless strain sensors because they are passive and economical to produce, especially, chip-less RF strain sensors that have several advantages over the active ones in terms of cost, simplicity, ability to operate in high-temperature environments, and printability with various conductive materials [71], [72]. Here, we discuss recent studies on printed wireless RF strain sensors.

In a recent study, Kim et al. [73] studied stretchable RFID for wireless strain sensing with silver nano ink. Flexible and stretchable LC resonator-based chip-less passive RFID tags have been fabricated by using the direct stamping method with silver nano ink. As demonstrated in figure 1.5.a, the LC circuit has a single-turn inductor connected to the inter digitated capacitor (IDC). By using a horn antenna connected to a VNA, a wireless readout of the RFID sensor has been provided. After stretching the RFID sensor, the gap between the fingers of the IDC has been increased and another dimension of the RFID sensor has been changed which results in a decrease in the resonant frequency as shown in figure 1.5.a.

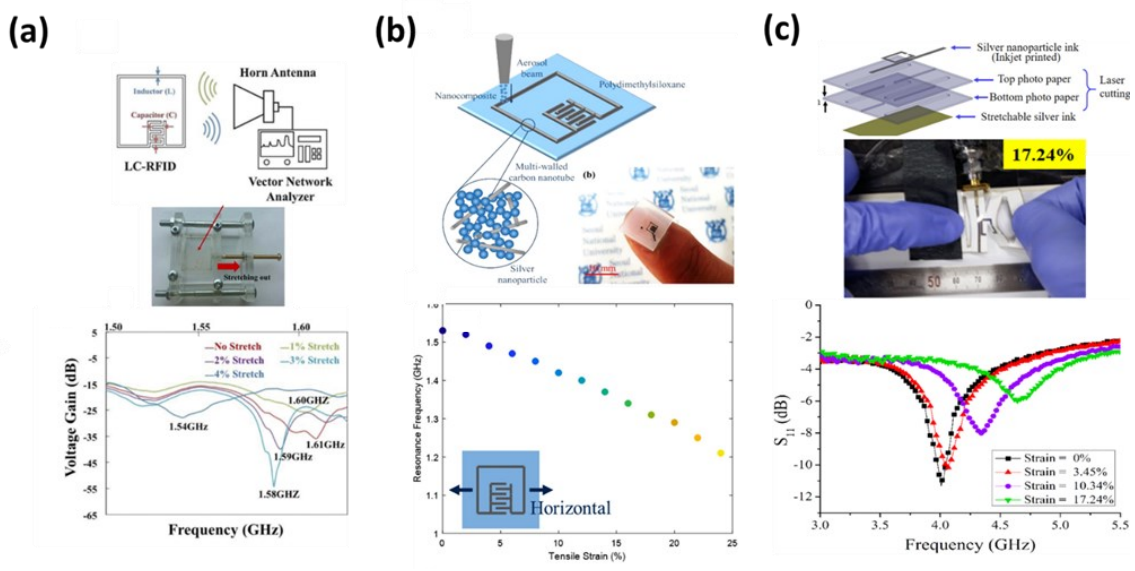

Figure 1.5. RF strain sensing. (a) Working operation of LC-RFID strain sensor and stretching test results. Reproduced with permission from ref. [73]. Copyright © 2014, IEEE. (b) Designed and printed LC resonance based passive RFID strain sensor and strain sensing results. Reproduced with permission from ref. [74]. Copyright © 2020, Elsevior. (c) Kirigami inspired split ring resonator (SRR) strain sensor stucture, strain experiment and results. Reproduced with permission from ref. [76]. Copyright © 2019, IOP Publishing.

In a similar way, Min et al. [74] demonstrated stretchable chip-less RFID multi-strain sensors using direct printing of aerosolized nanocomposite. They utilized multi-walled carbon nanotubes and silver nanoparticles as nanofillers in the nanocomposites. The RFID strain sensor was created by directly printing inorganic nanoparticles onto a stretchable, flexible substrate using an aerodynamically focused nanomaterial (AFN) printing system [75]. The nanomaterials placed in the nanomaterial feeder are aerosolized by aerodynamic shock induced by successive excitation and purging of compressed air. Figure 1.5.b shows the design and printed LC-based passive RFID strain sensor. A single-turn inductor and a capacitor with multi fingers have been used for generating resonance in an LC circuit. By applying a horizontal strain, the gap between the fingers of the capacitor increases, and the length of the inductor increases as well. The change in the diameters of the LC circuit causes the decrease in resonant frequency as demonstrated in the graph in figure 1.5.b. For using the sensor in different directions, they made a sensor with two different dimensions of LC circuit (different initial resonant frequency) and different orientations (90-degree difference) next to each other, so by applying a strain

horizontally and vertically, one LC circuit responses and its resonant frequency will change.

There are several different approaches for wireless RF strain sensor designs, which follow the theory of dependency of resonant frequency on geometrical changes because of the strain. For instance, Salim et al. [76] reported a kirigami-inspired split ring resonator (SRR) strain sensor. As demonstrated in figure 1.5.c, SRR resonance frequency is dependent on its split gap, a kirigami cut was designed to align with the SRR split gap, which allows SRR resonance frequency to be varied by applying tensile stress, which leads to strain. Two sheets of paper were used as the dielectric, and a conductive pattern was printed on the top paper using silver nanoparticle ink through ink-jet printing. Also, the ground plane on the bottom paper was inkjet-printed using stretchable silver ink. The 1.5.c shows that by applying more strain the resonant frequency of the sensor increases.

1.5.3. Temperature Sensing

The importance of temperature sensing in bio-medical, harsh industrial, and environmental applications has drawn the attention of several researchers [77]-[79]. In the meantime, several studies have been dedicated to wireless temperature monitoring sensors because of the potential application which requires wireless communication. For instance, it may be essential to check the internal temperature in a harsh sealed environment, and wireless readout of a regional body temperature is preferable to wired sensors in bio-medical applications [80], [81]. Among the wireless temperature sensing methods, RF temperature sensors have emerged in the past decade, especially using printing with conductive materials, because of the mentioned advantages in the previous applications.

Shao et al. [82] have reported a study on room-temperature high-precision printing of flexible wireless electronics based on MXene inks. They worked on a few RF sensors and tags with various applications such as strain and temperature. MXene is an additive-free titanium carbide ($Ti_3C_2T_x$) that can be used for printing conductive patterns [83]. As shown in figure 1.6.a, by using the DIW printing method, they printed an RF dipole antenna on polyethylene terephthalate (PET) and PDMS substrate, which can communicate wirelessly with a reader antenna. The communication procedure has been depicted in figure 1.6.a. By implementing a temperature reading chip to the RF dipole antenna they achieved real-time monitoring of temperature changes. For instance, they locally monitored the leaf surface temperature using four MXene RFID temperature tags mounted on the leaf surface and plant root, and the results are provided in the graph. In another example, MXene RFID temperature tags are used as wearable sensors to monitor surface temperature on the human wristband (inset), forehead, and chest. In another recent similar report, Pan et al. [84] have screen printed highly conductive graphene ink to make both near-field communication (NFC) antenna and far-field RFID antenna to use them with a temperature chip sensor as a wireless RF temperature monitoring sensor.

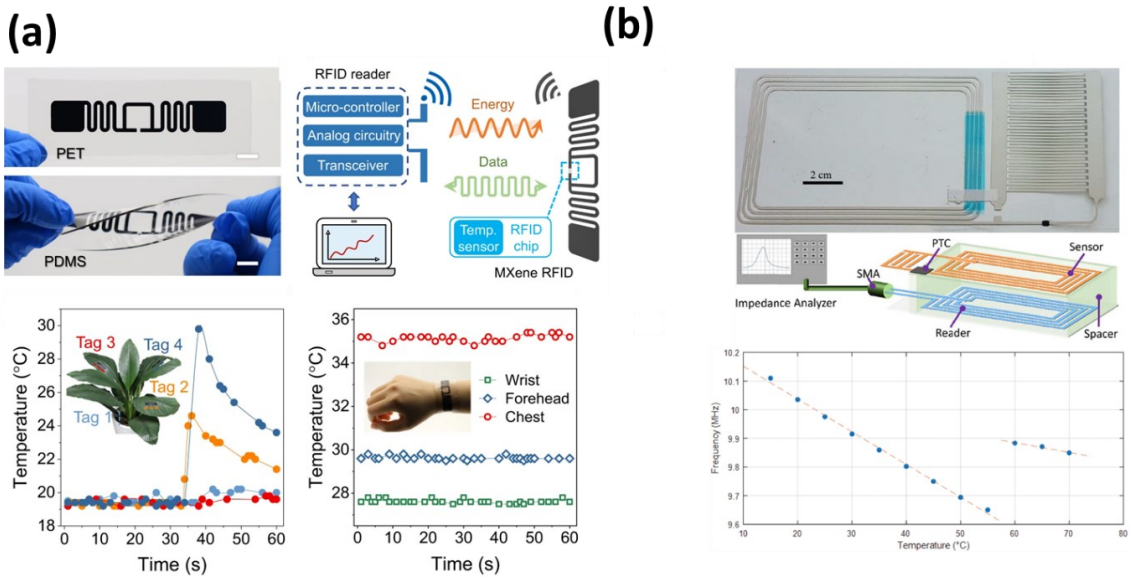

Figure 1.6. **RF temperature sensing. (a) RF dipole antenna on PET and PDMS substrate, working operations and temperature sensing results. Reproduced with permission from ref. [82]. Copyright © 2022, Nature. (b) Screen-printed chip-less RFID temperature sensor, working operation and results. Reproduced with permission from ref. [86]. Copyright © 2019, IEEE.**

So far, we outlined recent studies on wireless RF temperature sensors that utilized chips in their designs. There is another approach for temperature sensing which is chip-less wireless RF temperature sensing [85]. For instance, Albrecht et al. [86] designed a chip-less RLC (LC circuit with resistive element) temperature sensor as shown in figure 1.6.b. The sensor tag consists of a loop inductor and an inter digitated capacitor that are connected in parallel to form a resonant circuit with a signature resonance frequency. They used silver paste for screen printing elements and connections which provides high conductivity after thermal curing at 100°C for 30 minutes. To achieve temperature sensitivity, a short section of the connecting silver trace has been replaced by a thick layer of positive temperature coefficient (PTC) paste that increases its resistance with increasing temperature. The resonant frequency of the sensor decreases linearly with increasing the temperature up to 60°C. For a temperature higher than 60°C, the PTC sensor behaves as a series capacitance which reduces the total capacitance and causes a shift upwards in the resonant frequency as provided in the graph. In another study, Lu

et al. [21] reported bioresorbable, wireless, passive sensors as temporary implants for monitoring regional body temperature. They used an LC sensor with a temperature-dependent dielectric paste between the capacitor's electrodes. By altering the temperature, the dielectric constant changes which lead to changes in capacitance and resonant frequency. There are numerous studies in this matter using the same resonant frequency alternation theory, with different approaches that all of them accelerate the advances in temperature sensing technologies.

1.5.4. Biomedical Sensing

The goal to achieve enhanced diagnosis and to realize continuous monitoring of human health has led to a vibrant, dynamic, and well-funded field of research in medical sensing and biosensor technologies [87]. Physical and chemical sensor technologies are used in the large field of biomedical sensing to monitor and detect physiological parameters including heart rate, regional body temperature, blood pressure, regional body humidity, sweat pH level, etc [88], [89]. In the past decade, research groups have focused on wireless biomedical sensing technologies, especially RF printed sensors which are cost-effective, suitable for wearable devices, and have simple operation [90]. Figure 1.7.a demonstrates an example of an RF sensor patch with multiparameter sensing. The transponder includes a miniaturized antenna for energy harvesting and communication with a remote RF interrogator, a microchip for data sampling and signal modulation, and several sensing elements. The epidermal tag is printed on a bio-compatible membrane that may dynamically interact with the skin interface by absorbing bio-fluids such as sweat or releasing drugs and is suitable for ink-jet printing as a substrate. The resulting epidermal wireless RF sensor can perform different sensing of local skin features such as temperature, strain, sweat loss, and pH [91]. The sensing mechanism of physical parameters such as regional body temperature, strain, and pressure is similar to the previous sections that we discussed. Therefore, here we will introduce some studies in chemical input-based biomedical RF sensing applications.

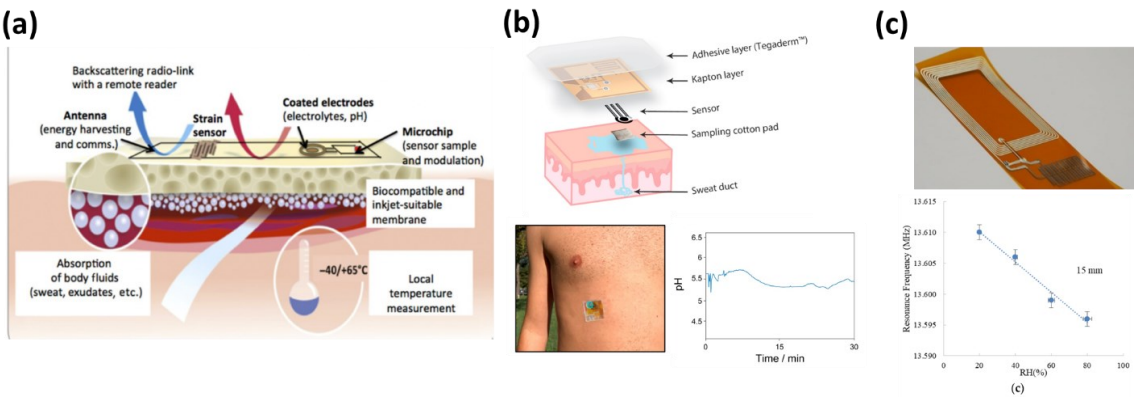

Figure 1.7. RF biomedical sensing. (a) An example of RF sensor patch with multiparameter sensing ability. Reproduced with permission from ref. [91]. Copyright © 2021, Elsevier. (b) Schematic of pH sensing elements, attached sensor to the human body and pH sensing results. Reproduced with permission from ref. [92]. Copyright © 2021, Elsevier. (c) Wireless chip-less LC humidity sensor and relative humidity measurement results. Reproduced with permission from ref. [95]. Copyright © 2018, MDPI.

Recently, Mazzaracchio et al. [92] reported a wireless and flexible epidermal device for pH monitoring in sweat, fabricated by enclosing a screen-printed potentiometric sensor, an integrated circuit, and an antenna embedded onto the same Kapton substrate. The integrated circuit board has been utilized for data acquisition and storage. In addition, a screen-printed RF identification antenna surrounding the entire system transmits the data to an external reader up to 2 meters. Figure 1.7.b shows a schematic of the different layers used to assemble the flexible device on the body for pH measurement. The conductive patterns have been screen-printed by a conductive ink, but for screen printing of the pH sensor element which is a three-electrode system, an Ag/AgCl ink has been used to print the pseudo-reference electrode and a graphite-based ink has been utilized to print the counter and working electrode. Finally, electrodes printed on Kapton were modified with iridium oxide by electrodeposition. As depicted in figure 1.7.b, a cotton pad has been placed beneath the electrochemical pH sensor to collect the body sweat from the skin and wet the sensor electrodes. The sensing mechanism is an ion exchange between the sweat and electrodes which leads to the potential (V) change. The graph demonstrates a real case experiment of the sensor attached to the human body for real-time measurement of the pH of the sweat.

Humidity is one of the key factors in wound monitoring. Finding the moisture or the humidity can help in analyzing the condition of a wound's healing to monitor the healing process [93]. There are several studies on wireless humidity sensor tags that can be used inside the patch or band-aids to find the relative humidity of the injured area wirelessly [23], [90], [94]. Printed humidity RF sensors are a proper candidate for wound monitoring because of their advantages in previous applications. For instance, Salmerón et al. [95] reported a wireless chip-less LC sensor for humidity sensing. As shown in figure 1.7.c, they designed an LC circuit with a coil inductor which was printed by silver conductive paste, and a capacitor consisting of 12 replicas of interdigitated electrodes (IDE) that ink-jet printed by silver nanoparticle ink. The ink-jet printing method allows the reduction of the distance between consecutive fingers and, therefore, increases the sensitivity of the sensor without occupying more area. The sensing mechanism is the monitoring of capacitance change by having a different relative humidity. In particular, the electrical permittivity of the selected substrate changes with the moisture content. Therefore, variations in RH produce changes in the capacitive value, inducing a shift in the resonant frequency of the chip-less sensor tag. The graph in figure 1.7.c shows the resonant frequency changes with different relative humidity at a 15 cm distance between the reader antenna and the sensor tag. Recently, many studies have been conducted dedicated to humidity and moisture sensing of the human body or wound area by using printed RF sensors. Most of them utilize the same sensing method with different designs and materials [96]-[98].

1.5.5. Chemical Sensing of Environment

Monitoring the environment in which we are living becomes gradually important, because of its direct impact on the quality of our life [99]. Studies on wireless environmental sensing systems have intensified in the last decade due to the growth of IoT technologies. As a result, RF sensing methods with applications for environmental sensing have been the subject of several studies [100], [101]. Environmental sensing is a comprehensive field of study that consists of physical sensing and chemical sensing. For instance, temperature sensors can be considered in physical parameter sensing of an open or closed environment. Here, we summarize chemical sensing in different aspects such as ion sensors, gas sensors, and humidity sensors in an environment.

Among the vast area of environmental sensing, ion sensors play an important role in the quality monitoring of an aqueous environment [102]. Recently, studies in this matter pave the way for future advances in this area. For illustration, we will overview the recent study from Kim et al. [19] on 3D-printed disposable wireless ion sensors. They reported different properties of prepared nanocellulose-based inks composed of silver nanowires (AgNW) as conductive fillers and cellulose nanofibers (CNF) or cellulose nanocrystals (CNC) as environment-friendly matrix materials. These conductive inks have been used for DIW 3D printing of sensing devices. As demonstrated in figure 1.8.a, their designed and fabricated sensor consists of an ion-selective membrane electrode (ISME) integrated into an LC circuit to provide the RF data for wireless communication to the reader. The sensor has a specific resonant frequency, and its intensity (Q factor) depends on the resistance of the closed-loop circuit. By monitoring different ion concentrations in the soil through the ion-selective membrane, the resistance of the closed-loop RF sensor changes. The primary ion of an ion-selective membrane is the ion that is targeted to be selectively detected by the membrane, while nonprimary ions are all other interference ions different from the primary ion. An ISME has a lower resistance if the relevant primary ions are moved through the ion-selective membrane because primary ions can move through the relevant selective membrane while nonprimary ions cannot [103]. An extracted soil droplet that has a different concentration of NH_4^+, K^+, and Ca_2^+ ions is applied to the ISME electrode. As shown in the graph, when the concentration of NH_4^+, K^+, and Ca_2^+ ions increase from 0.5 to 2 M, the Q factor at the resonant frequency also changes. The sensor has a higher sensitivity for the primary ion, NH_4^+. Therefore, by utilizing the desired ISME in this sensing system, the targeted ions can be detected in liquid samples which can have vast applications such as soil ion or water quality measurements [104].

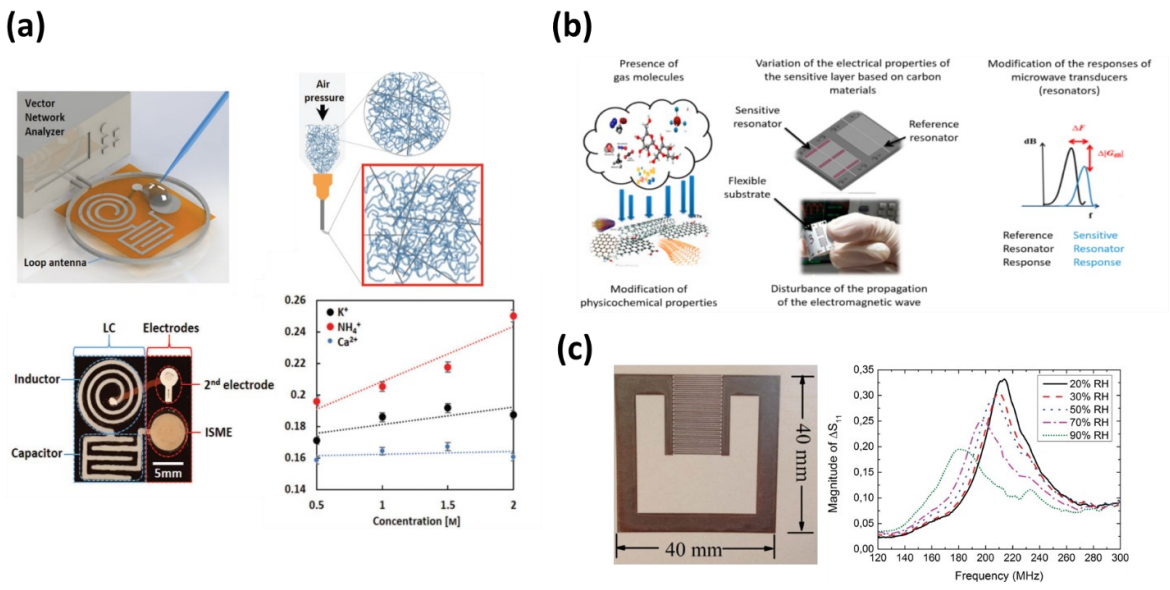

Figure 1.8. **RF Environmental sensing. (a) Wireless ion detection system, DIW printing of CNF-AgNW ink, printed sample of IS-LC sensor and experimental result of IS-LC sensor with NH4 membrane. Reproduced with permission from ref. [19]. Copyright © 2018, WILEY-VCH Verlag GmbH & Co. KGaA. (b) Summary of the operation and sensing process of carbon nanotube-based RF volatile organic compounds (VOC) gas sensor. Reprinted with permission from ref. [107]. Copyright © 2019, MDPI. (c) Chip-less RFID sensor tag for environmental humidity sensing and relative humidity sensing results. Reproduced with permission from ref. [113]. Copyright © 2015, IEEE.**

Another important factor in the environmental sensing area is gas concentration measurement and monitoring in a particular environment. Recently, several studies have been dedicated to the design and fabrication of wireless RF gas sensors [105], [106]. For instance, George et al. [107] reported a carbon nanotube-based RF volatile organic compounds (VOC) gas sensor. Figure 1.8.b shows a summary of the operation principles and sensing process. They designed an RF sensor with two different electromagnetic resonators to have two signatured resonant frequencies: A gas sensitive resonator, and a reference resonator. Ink-jet printing with silver nanoparticles on a paper substrate has been used for the fabrication of resonators. Two resonators have the same design consisting of two parallel networks of 50 electrodes. The sensitive resonator has 5 layers of multi-wall carbon nanotubes (MWCNTs) embedded in poly (3,4-ethylene

dioxythiophene) polystyrene (PEDOT: PSS-MWCNTs) as sensitive material for VOC gas detection. By applying various concentrations of the ethanol gas to the sensor, the permittivity of the sensing resonator changes because of the reaction between the ethanol and MWCNTs. Therefore, the resonant frequency of the sensing resonator changes whereas the resonant frequency of the reference resonator doesn't affect by the gas. By finding the difference between two resonant frequencies, they could find the concentration of the applied gas. By using the same approach, RF resonators have the potential to detect gas concentration in a specific environment [108], [109].

Humidity or moisture sensing in an environment is crucial in many fields such as agriculture, industrial laboratories, and even air quality in a closed environment such as a home or workplace [110], [111]. Several studies on the development of humidity or moisture sensing have been demonstrated in the past decades. Printed RF humidity sensors have been investigated thanks to their cost-effectiveness and simplicity. In most cases, the sensing mechanism is changing the resonant frequency of the sensor affected by the relative humidity of the sensor environment [53], [112]. For example, figure 1.8.c shows an RFID sensor tag designed and fabricated by Feng et al. [113] consisting of a single-turn inductor and an IDC. The sensor is ink-jet printed with silver nanoparticle ink on a PET substrate. By increasing the relative humidity of the environment that the sensor is placed in, the permittivity of the dielectric (air) between the IDC electrodes increases, leading to an increase in the capacitance and a decrease in the resonant frequency as shown in the graph. Several reports in this area have been reported in the past few years which help the development of humidity sensing areas.

Chapter 2. New Device Design and Fabrication

2.1. Conventional Designs of Wireless LC Sensor

LC sensors consist of an inductor (L) and a capacitor (C) which are connected to each other and are in resonance with each other. Each sensor has its own resonant frequency which has a relation with its inductance and capacitance. In order to detect the resonant frequency of an LC sensor, an external readout coil which is connected to a VNA will be placed on top of the sensor, to interact with the magnetic field that comes from the inductor of the sensor. The readout coil will have a mutual inductance with the inductor of the sensor, therefore the signatured signal directly related to mutual inductance can be transferred from the sensor to the VNA as explained in section 1.3.1. The resonant frequency of an LC sensor with a capacitance of C_S and Inductance of L_S is expressed in equation 1.1. There are three main approaches for designing an LC sensor which will be discussed.

2.1.1. Separated Inductor and Capacitor

A conventional design of an LC sensor is a separated inductor and capacitor connected to each other. As an example, figure 2.1 demonstrates the design of a wireless LC humidity sensor consisting of an IDC connecting to a rectangular coil inductor [114]. Although this type of design allows us to separately choose the shapes and dimensions of the inductor and capacitor, however, because of the separation there is a limitation for decreasing the size of the sensor and making the sensor compact which is required in several applications. Additionally, since this type of design is anisotropy, the mechanical behavior of the sensor varies in different directions which can affect the resonant frequency by applying mechanical loads.

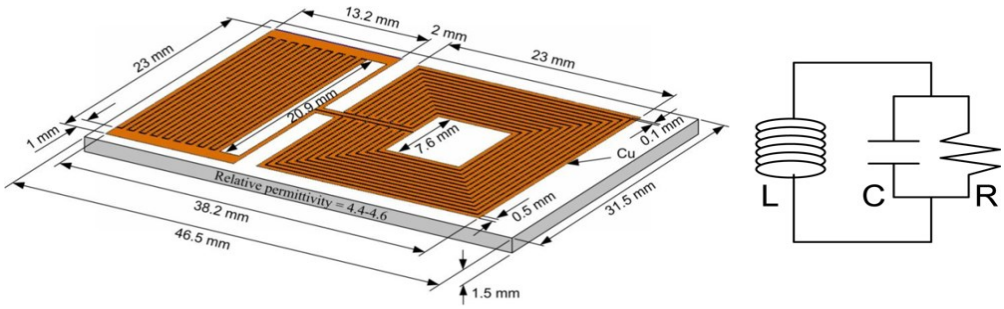

Figure 2.1. A separated design of a wireless humidity sensor. Reprinted with permission from ref. [114]. Copyright © 2010, MDPI.

2.1.2. Rectangular Design

For achieving a more compact sensor, many reports demonstrated a rectangular design of the LC circuit in a way that the capacitor is placed in the middle of an inductor coil. For instance, Tan et al. [115] reported a wireless passive sensor for quantifying packaged food quality. Figure 2.2 shows the rectangular design of the LC sensor and the steps of completion of the connection between the coil inductor and the capacitor. These types of circuit design for LC sensors are good candidate for applications that requires compact sensors. However, having sharp edges increase the probability of disconnection of the inductor coil or capacitor's electrodes. Additionally, these sensors suffer from anisotropic behavior of mechanical properties.

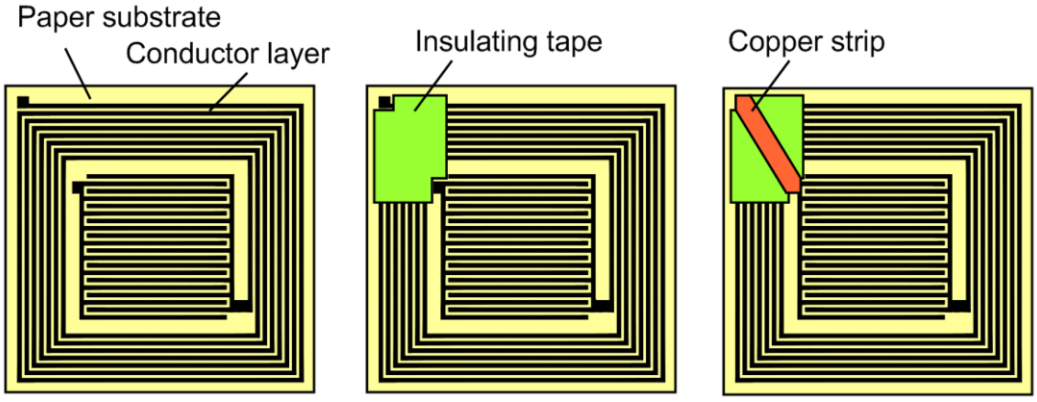

Figure 2.2. Rectangular design of a wireless sensor. Reprinted with permission from ref. [115]. Copyright © 2007, MDPI.

2.1.3. Stacked Design

Another conventional design for wireless LC sensors is a stacked or multilayer design. There are several studies on wireless LC sensors with a stacked design which is usually designed for pressure sensing. For example, Nie et al. [116] reported a textile-based wireless LC pressure sensor. Figure 2.3 depicts the design of the LC circuit and final pressure sensor. As shown in figure 2.3, the pressure sensor consists of several layers such as a planar coil, IDC, spacer, and a ferrite film. Although these types of multilayered designs show a reliable performance in pressure sensing applications, because of the large thickness they can not be utilized in embedded systems, and most of them require several steps of fabrication and electrical connections between different layers.

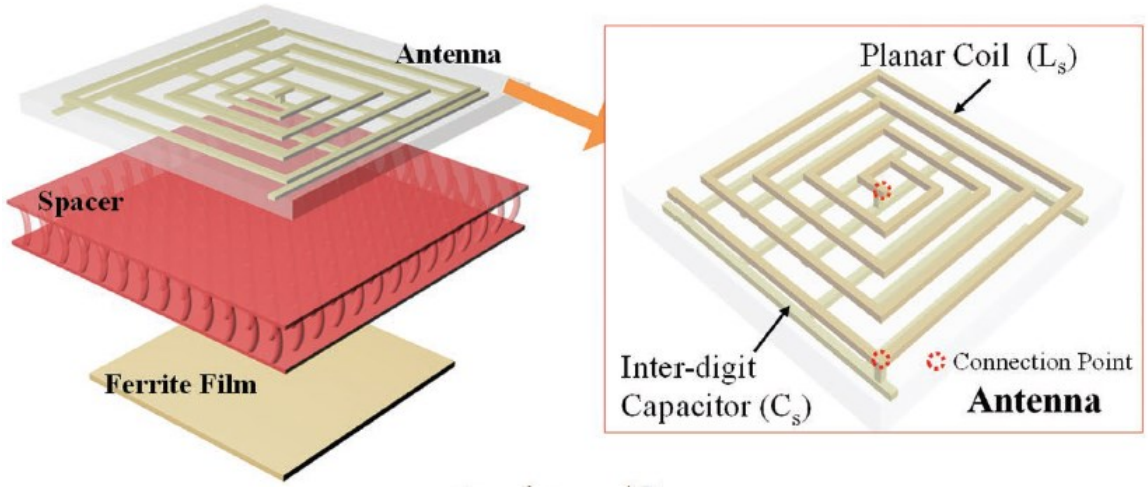

Figure 2.3. Stacked design of a wireless LC pressure sensor. Reprinted with permission from ref. [116]. Copyright © 2019, WILEY-VCH Verlag GmbH & Co. KGaA.

2.2. Compact Design of LC Sensors

As a means of achieving sensors with different resonant frequencies, three compact sensors with differing capacitance have been designed. As shown in figure 2.4, three sensors have 3.75 turns of the inductor on the outside which is connected to the curved and interdigitated capacitor at the center. The width of the inductor turns, and each finger of IDC is 300 μm, and the gap between the inductor's turns and the capacitor's fingers is 300 μm. The outer diameter of the sensor is 18 mm. For having differing capacitance in three sensors, a different number of paired fingers of the capacitor has been selected. LC sensor number 1 has two pairs of curved electrodes, LC sensor 2 has three, and LC sensor 3 has four pairs of capacitor electrodes. By having a greater number of paired fingers of the capacitor, capacitance is increased, therefore based on equation 1.1, the resonant frequency is decreased.

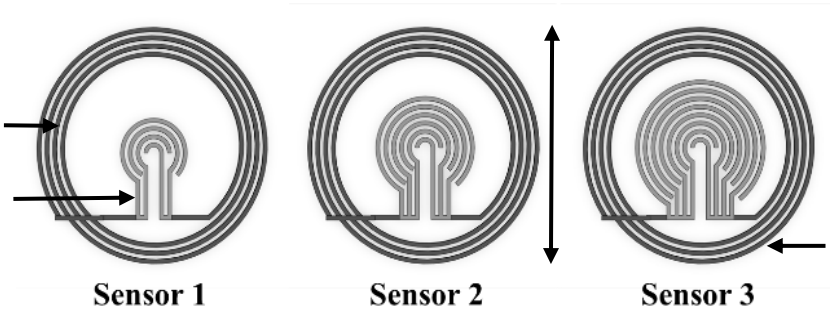

Figure 2.4. Proposed design of three different LC sensors with their dimensions.

Both inductors and IDC capacitors have been designed as circular shapes to achieve a fully compact design without any sharp edges. The number of inductor turns, and the capacitor fingers have been controlled to achieve a resonant frequency in the range of 1-4 GHz as a demonstration. So, three sensors will have three different resonant frequencies based on equation 1.1, which is required to distinguish each sensor in different locations to achieve multiple location sensing in the desired application. Circular designs of the LC sensors demonstrate reliable mechanical behavior which leads to consistent electromagnetic behavior depending on the strain change. The demonstration of the mechanical behavior of designed sensors is provided in the finite element analysis (FEA) section.

2.3. DIW-based 3D Printing of LC Sensors

For having a closed LC circuit, the inductor must be connected to both electrodes of the capacitor. Since an inductor is outside of a capacitor in the proposed design, a bridge between the inductor and the capacitor is required to complete a closed circuit. Figure 2.5.a shows the DIW-based 3D printing method for the fabrication of an LC sensor with a bridge for connecting the capacitor to the inductor, so the circuit can be closed. This ability of DIW-based 3D printing that allows printing a bridge on top of the inductor in a different layer, will make the process of fabrication faster than constructive methods and helps to save conductive material. A 3D computer-aided design (CAD) model of LC sensors has been designed and converted into a tool path, and the 3D printer moves the nozzle based on the designed tool path. By applying pressure to the syringe, the conductive ink is dispensed from the nozzle and makes the desired path. Parameters like dispensing pressure, the movement speed of the nozzle, and the distance between the nozzle and the surface determine the width and quality of printed patterns.

The printed sample has been shown in figure 2.5.b, in which the bridge area is focused. The DIW printer is ML-808 GX by Musashi Engineering. The conductive ink that has been used is “Voltera’s conductor 2 ink” which has a resistivity of 1.265×10-7 Ωm. After printing the LC sensors with conductive ink on a polyimide substrate, samples have been cured thermally at 120 °C for 30 minutes to achieve fully dried and conductive traces.

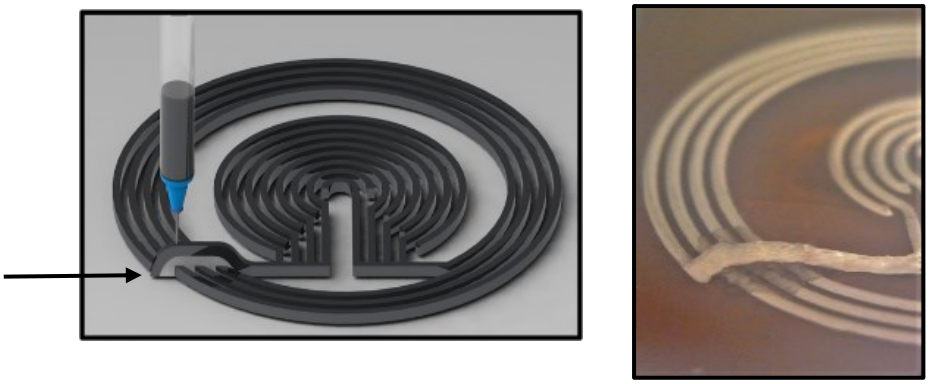

Figure 2.5. DIW 3D printed LC sensor (a) Schematics of 3D printing process for the fabrication of LC sensors. (b) Actual sample image of the 3D printed bridged structure.

Chapter 3. inite Element Analysis

3.1. FEA Simulation of LC Sensors

For finding resonant frequencies of the LC sensors by experiment, an external readout coil is employed. The coil antenna is connected to the SMA (Sub Miniature version A) adapter and then connected to the VNA with a cable. The SMA connector has an impedance of 50 Ω and is designed to function in the frequency range of 0 to 12 GHz. The resonant frequency of the sensor is obtained via electromagnetic coupling between the readout coil and the inductor of the LC sensor. For one port measurement system with the coil antenna, the input return loss (S11) parameter or reflection coefficient is measured in the desired frequency range. The frequency in which S11 is the minimum is close to the resonant frequency, therefore with this method resonant frequency of the LC can be measured.

In this study, finite element analysis that mimics the real experiment situation has been conducted for the characterization of LC sensors for the validation and characterization of the sensor design. ANSYS HFSS (High-frequency structure simulator) has been utilized for the S11 simulation of the resonant frequencies of LC sensors. The conductive material used in the simulation setup for sensors is bulk silver with a resistivity of 1.6×10^{-8} Ωm.

Figure 3.1.a shows the ANSYS HFSS interface of the simulation setup. A circular coil antenna of 2 cm diameter has been connected to the SMA and placed on top of the LC sensor with 4 mm. After conducting a simulation, the S11 coefficient has been found in different frequencies. The plot of S11 versus frequency has been obtained as shown in figure 3.1.b. The blue line is for LC 1 which has two pairs of capacitor fingers, showing that the minimum value of S11 is around 2.76 GHz which can be indicated as the resonant frequency of LC 1. The orange line is for LC 2 with three pairs of capacitor fingers, showing that the resonant frequency is around 2.74 GHz. The red line is for the LC 3 with four pairs of capacitor fingers, showing that the resonant frequency is around 2.72. Results show that three sensors have distinct resonant frequencies. Moreover, since LC 1 has the minimum capacitance among other sensors, it has the highest resonant frequency, and LC 3 has the lowest resonant frequency among them because of its maximum capacitance in line with the theoretical expectation from equation 1.1.

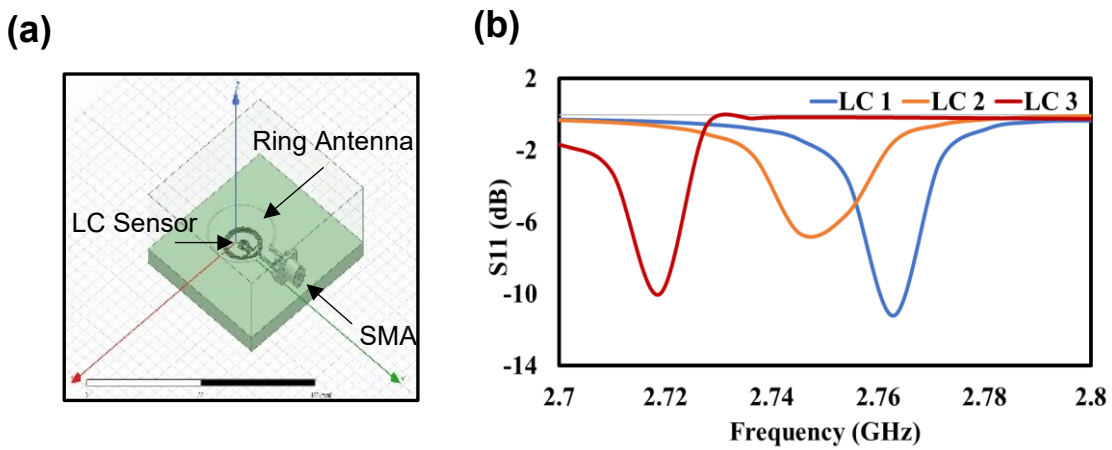

Figure 3.1. FEA simulation of designed LC sensors. (a) Ansys HFSS simulation interface for the validation of designed sensors. (b) S11 simulation results for resonant frequency of three LC sensors.

Figure 3.2 shows the simulation results of resonant frequency changes in applied strain for LC sensor 3. Thanks to the circular shape of the LC sensors, the resonant frequency does not change drastically by applying the strain in both the x and y directions up to 0.5%. This isotropic behavior can be useful in various applications in which some unwanted strain might occur and won't affect the resonant frequency.

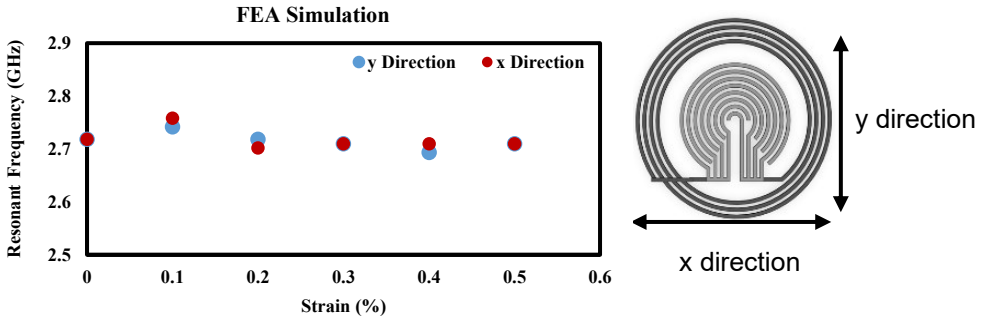

Figure 3.2. Resonant frequency of LC sensor 3 with horizontally and vertically applied strains.

3.2. FEA Simulation of RF Sensor Tag

To find the resonant frequency with different location information, the transmission coefficient (S21) is measured in the desired frequency range. The frequency in which S21 is minimum is close to the resonant frequency. For the integration of the designed LC sensors and RFID communication, an RF tag is needed. For the simulation of transmission coefficient (S21), sensors with polyimide substrate have been placed on top of the L shape transmission line (strip line) with 3.5 mm width on top of the printed circuit board (PCB) substrate, as shown in figure 3.3.a in a way that their inductors cover the strip line and communicate with the strip line with mutual inductance. The length of the L shape tag is 105 mm, and the width of the tag is 75mm. A copper plate has been attached at the bottom of the PCB which acts as a ground. The tag dimensions and locations of LC sensors have been optimized by FEA simulation and provided in appendix A. Signals from the first port move along the strip line and the signatured signal which has the information of the LC sensor will be transferred back to VNA via the second port for analysis.

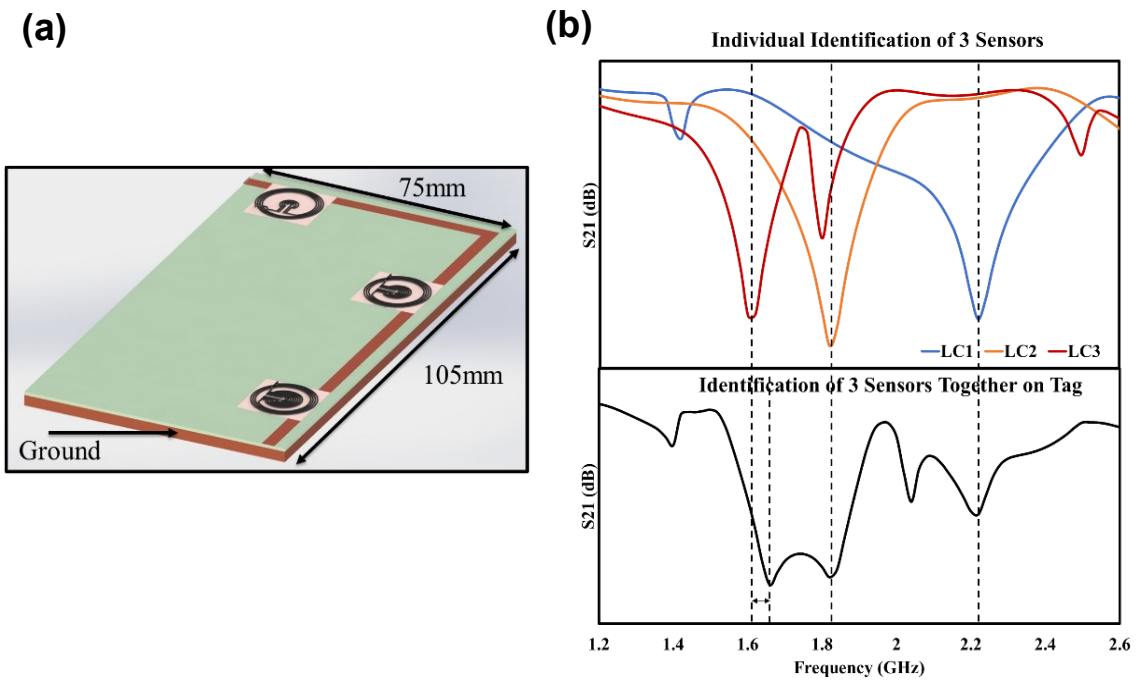

Figure 3.3. RF sensor tag design and simulation. (a) Three LC sensors on top of the strip line. (b) S21 simulation results of three LC sensors on the tag (top: individual sensor, bottom: three sensors together).

For the simulation, each sensor has been put on the strip line individually, and results have been collected first. Furthermore, three sensors have been put on the strip line together, and results have also been collected as shown in figure 3.3.b. For the individual case, LC 1 has a resonant frequency of 2.22 GHz. Resonant frequencies of LC 2 and LC 3 are 1.82 GHz and 1.61 GHz respectively. Results from the bottom graph which is for all LC sensors together on the transmission line show that for LC 1 and LC 2, resonant frequencies match the individual cases, and the difference in resonant frequency is around 50 MHz for LC 3, which may come from the interaction among the magnetic fields of three sensors. All LC sensors still can be identified individually. Moreover, the discrepancy between the S11 and S21 results comes from the difference in mutual inductance between LC sensors and coil antenna in the S11 measurement, and the mutual inductance between LC sensors and transmission line in the S21 measurement. From S11 and S21 measurements, it has been confirmed that each sensor has its own resonant frequency which varies from other sensors, therefore when each sensor is placed at a different location it has its own specific location-based information that is different from other locations with a sensor.

3.3. FEA Simulation of Dielectric Material Effect

So far, The LC sensor with a thin polyimide substrate has been placed directly on top of the strip line and the FEA simulation has been conducted. Here we want to place different materials between the LC sensor and the strip line and find their effect on communication between the LC sensor and the strip line. To find the effect of the dielectric constant of dielectrics on communication between LC sensors and strip line, FEA simulations with ANSYS HFSS have been conducted for four different dielectric materials and thicknesses ranging from 1 to 5 mm. The simulation setup interface in ANSYS has been shown in figure 3.4.a, and the relative permittivity (dielectric constant) of four dielectric materials has been provided in table 3.1. Figure 3.4.b shows the S21 result with different dielectric material thicknesses for PMMA, Epoxy, Al_2O_3, and TiO_2 in the case of LC 3.

Table 3.1. Relative permittivity of four dielectric materials.

Dielectric Material	Relative Permittivity
TiO_2	86
Al_2O_3	9.8
Epoxy	4.4
PMMA	3.4

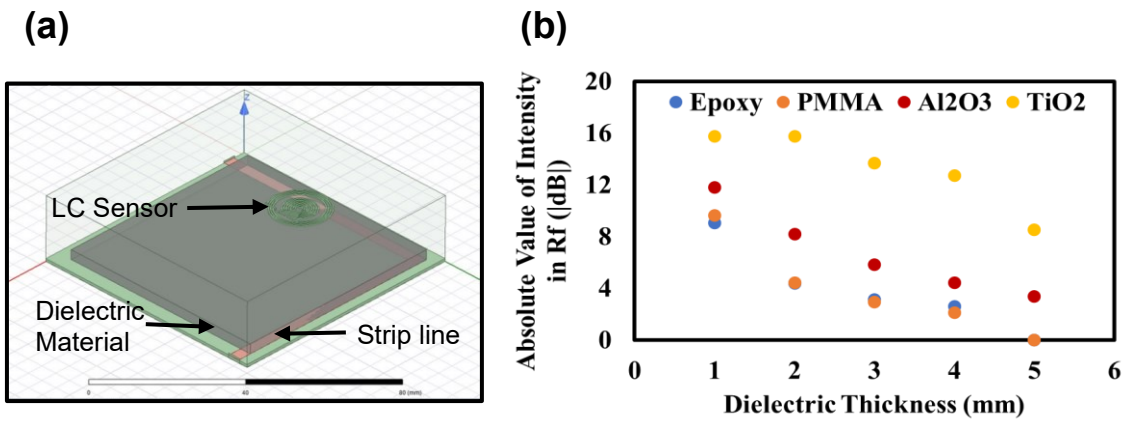

Figure 3.4. FEA simulation of dielectric material effect. (a) Simulation setup interface in ANSYS HFSS. (b) Simulation results of dielectric effects on intensity of S21 coefficient in resonant frequency for LC sensor 3 in different thickness of dielectric material.

As shown in the graph, by increasing the thickness of the dielectric material, the intensity of S21 decreases. For PMMA and Epoxy, the intensity of S21 goes to 0 with a thickness over 4 mm, which means that the resonant frequency cannot be found. From table A1 in appendix A, the dielectric constants of PMMA and Epoxy are 3.4 and 4.4 respectively. With the Al_2O_3, which has a dielectric constant of 9.8 (higher than PMMA and Epoxy), it has more permittivity, so the magnetic field from an inductor of the sensor can reach the strip line, and they can communicate up to 5 mm thickness of the Al_2O_3.

Another dielectric material that has been chosen for this part is TiO_2 because of its high dielectric constant which is 86. As shown in Figure 5a, for TiO_2 as a dielectric between the LC sensor and strip line, the intensity of the S21 coefficient in the resonant frequency of the sensor is much higher than other materials from 1 mm to 5 mm of thickness. Its high permittivity allows proper electromagnetic communication between the LC sensor and the strip line.

3.4. Conclusions

By utilizing the FEA method, the simulation of the designed LC sensors and the RF tag has been conducted using ANSYS HFSS. First, it has been confirmed that three compact LC sensors show different resonant frequencies owing to the difference in their capacitance. Next, by applying strain in two directions, the resonant frequency did not change significantly. Moreover, by simulating the RF sensor tag with three LC sensors on the strip line, the communication between LC sensors and the strip line has been confirmed. Three compact LC sensors show different resonant frequencies on the RF tag. Finally, by using different dielectric materials between the strip line and LC sensors, the effect of dielectric materials on the resonant frequency and communication has been studied and discussed.

Chapter 4. Experimental Analysis

4.1. Verification of Fabricated Sensors

After we confirmed the FEA simulation, an experimental method has been chosen to verify the communication between LC sensors and the strip line. As shown in Figure 3a, L type strip line has been fabricated on top of the tag with a 3.5 mm width of copper sheets as a transmission line. Two ends of the strip line have been connected to SMA connectors. On the other side of the tag, a copper plate has been used to act as a ground. Two SMA connectors have been connected to the VNA input and output ports for conducting the measurement of the S21 coefficient. The VNA that has been used in this study is the "Rohde and Schwarz ZND Vector Network Analyzer" with a frequency range of 100 kHz to 4.5 GHz.

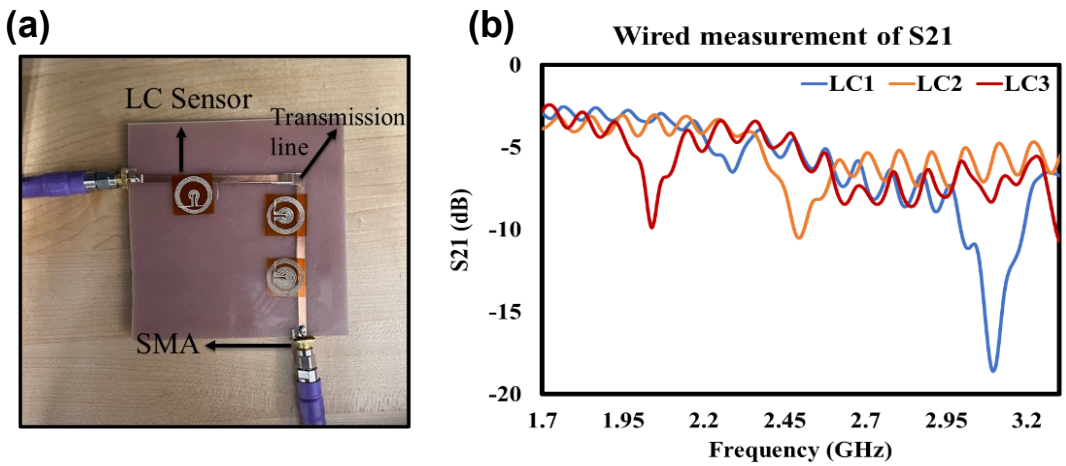

Figure 4.1. Experiment confirmation of fabricated sensors. (a) Actual image of wired S21 measurement of three LC sensors placed on top of the strip line. Port 1 is connected to VNA and receives the signals and Port 2 transfers the signals back to the VNA. (b) Results from S21 wired measurement using SMA and strip line.

One sensor at a time has been placed on top of the strip line in a way that its inductor is placed exactly on top of the strip line so that they can have mutual inductance between

them. After completing the setup, the VNA applied the excitation from one port and received the signal from another port. The S21 graph has been obtained as shown in Figure 3b. The blue line is the result of putting LC 1 on the strip line, the orange line is for LC 2, and the red line is for LC 3. All three results from three sensors have been shown in one graph for comparison of three sensors. The minimal number of S21 coefficients for LC 1 is in 3.09 GHz frequency which is considered as its resonant frequency. LC 2 has a resonant frequency of 2.48 GHz, and the resonant frequency of LC 3 has been found 2.05 GHz.

The behavior of decreasing resonant frequencies by having a sensor with a larger capacitance has been proved by the S21 measurement. It has been expected that results from the experiment don't completely match the results from the FEA simulation because the properties of the material used in fabrication are different from the material parameters used in the simulation. For instance, the conductivity of the silver conductive ink used for the fabrication is different from the conductivity of bulk silver in the FEA simulation.

4.2. Wireless Sensor Characterization Setup

Figure 4.2.a shows a schematic of the wireless detection system. Signals come from one port of the VNA which leads to the transmitter (Tx) reader antenna. This antenna transmits the signal from one side, and the receiver (Ry) tag antenna which is connected to the strip line receives the signals. This Ry tag antenna transmits the signals to the strip line, and signals go through the strip line while LC sensors placed on top of the strip line sign the signal with their resonant frequencies. Signatured signals go through the transmitter (Ty) tag antenna, and this antenna transmits the signal to the VNA receiver (Rx) reader antenna and then to the VNA to collect the signals for the S21 versus frequency graph.

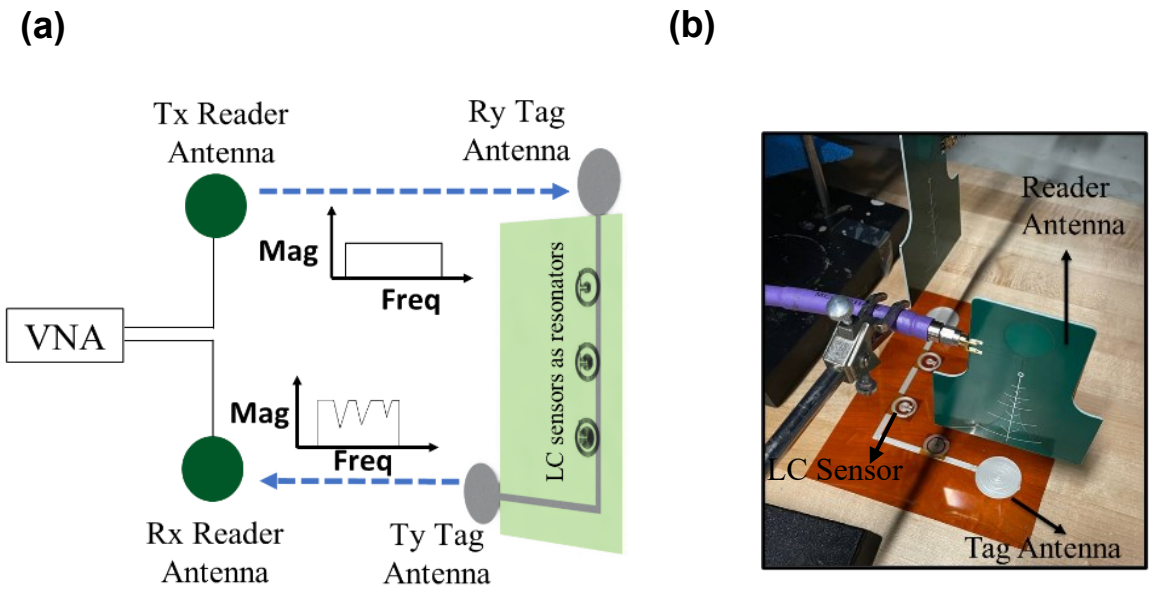

Figure 4.2. Wireless sensing setup. (a) Schematic of wireless measurement setup consists of reader, sensor tag and antennas. (b) Actual image of wireless experiment setup.

The photo image of the experimental setup is shown in figure 4.2.b. The tag size is 105mm by 75mm. Commercial antennas have been used as reader antennas, and monopole antennas with a diameter of 3 cm have been printed as tag antennas. A tag that has L type strip-line and two monopole antennas have been fabricated by DIW-based 3D printing method with conductive ink on top of a polyimide substrate, then thermally cured to be fully conductive, and finally attached to a copper plate ground on the other side.

4.3. Experimental Results of Wireless RF Sensing

After setting up the wireless sensing setup as discussed in 4.2, the wireless experiment has been conducted. Figure 4.3.a shows the results of putting one sensor at a time on top of the strip line for a working distance of 5 mm. As shown in the graph, the resonant frequencies of the three LC sensors are different from each other and distinguishable, and the tag without any sensors shows wireless communication. From the graph, LC 1 has a resonant frequency of 3.69 GHz, LC 2 has a resonant frequency of 3.61 GHz, and the resonant frequency of LC 3 is 3.49 GHz. The same experiment has been conducted for LC 1 at different working distances from 1 to 10 cm. Resonant frequencies of tags without LC sensors and with LC 1 in different working distances have been collected from the S21

versus frequency graphs as shown in figure 4.3.b. For each working distance, signals were detectable, and the resonant frequency has been found from the S21 versus frequency graph. For the working distance beyond 10 cm, it was hard to distinguish a minimum S21 for finding the resonant frequency of the sensor, which means that the proposed system with these types of antennas has a maximum working distance of 10 cm, which is a significant improvement in case of working distance of LC sensor by itself.

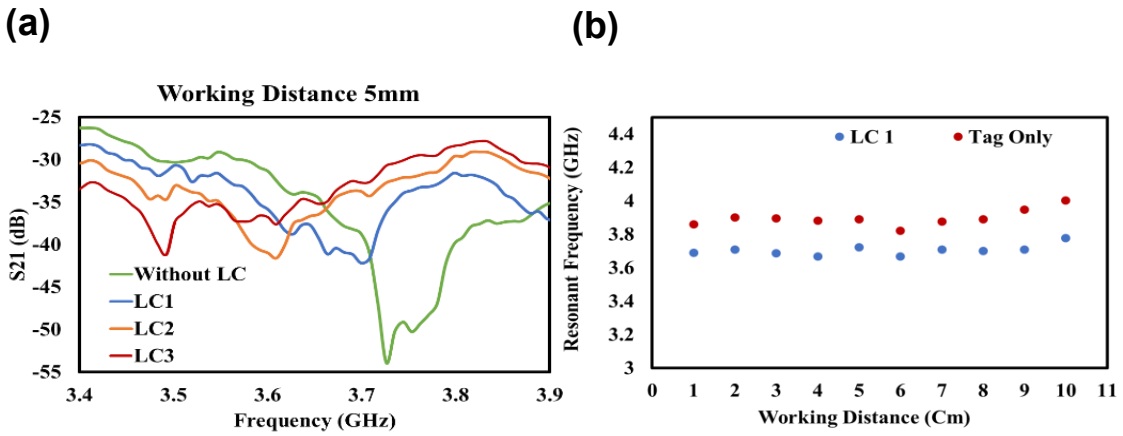

Figure 4.3. Wireless sensing experiment. (a) Results of wireless S21 measurement of the sensor tag with 5mm working distance. (b) Results from S21 measurement of tag without sensor and with LC sensor 1 for ten different working distances.

4.4. Sensing Performance with High Dielectric Material

In section 4.3, LC 1 has been used for wireless measurement at different distances between tag and VNA transmitter and receiver antennas. Figure 4.4 shows the schematic of the wireless setup with different working distances. As wireless measurement has been conducted for LC 1, it has been noticed that finding a resonant frequency for a relatively longer working distance (> 6 cm) is challenging, and the bandwidth at the resonant frequency increased, which means the quality factor is decreased by increasing the working distance.

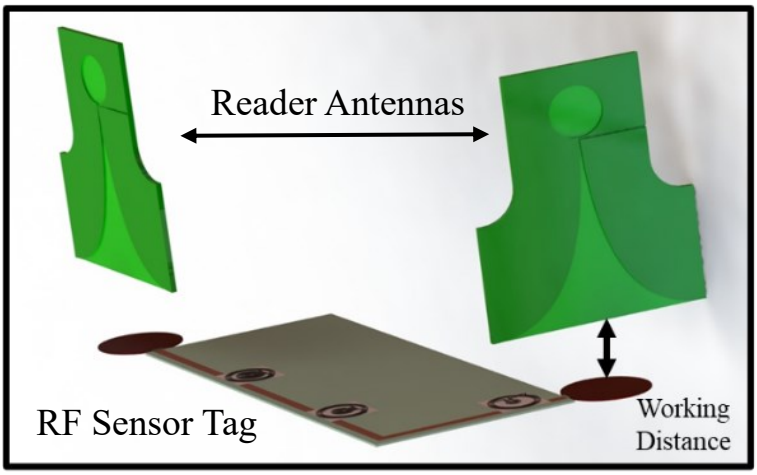

Figure 4.4. Wireless setup schematic illustrating the working distance.

For enhancing the quality of wireless communication between the RF sensor tag and the reader, the dielectric material paste that contains TiO_2 has been prepared, and after applying it to the sensor, its effect on wireless communication has been studied. For making the 3D printable dielectric paste, Urethane Triacrylate oligomer was mixed with NFC with Phenylbis phosphine oxide as a photo-initiator. This paste is UV curable by light with a wavelength of 400 nm.

After making the paste, 40 wt. % of the TiO_2 powder has been added to the paste, and the paste was mixed with a speed mixer to achieve a homogeneous 3D printable paste. TiO_2 has been chosen because of its high dielectric constant and permittivity to make a dielectric paste with a high dielectric constant. The dielectric constant of the paste has been measured for different wt. % of TiO_2 and the results have been provided in figure 4.5.

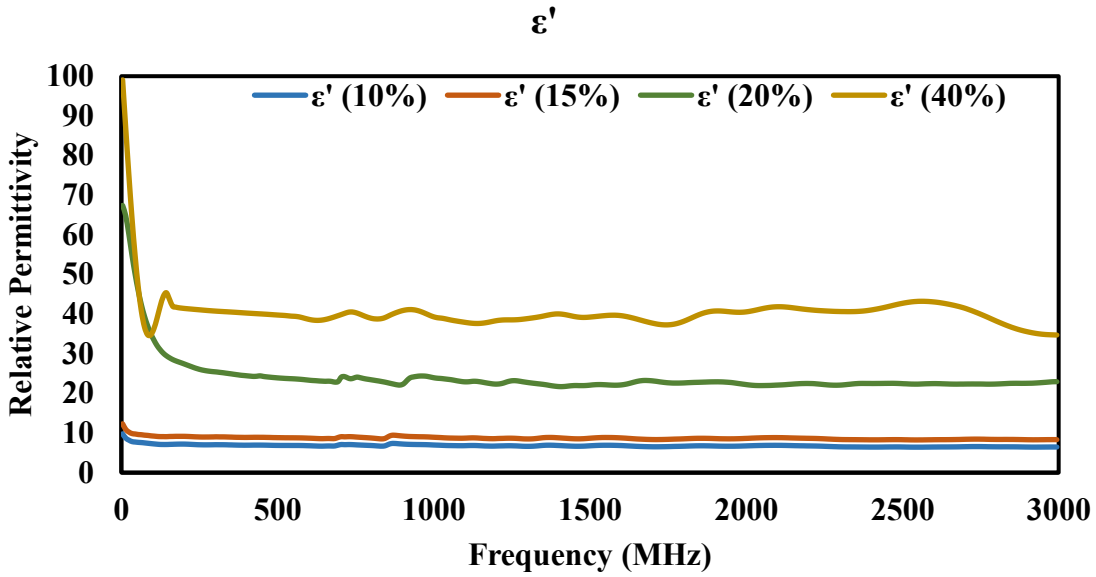

Figure 4.5. Dielectric constant measurement results for dielectric paste with different wt. % of TiO_2.

For the paste with 40 wt. % of TiO_2, the measured relative permittivity is around 43, therefore this dielectric paste has been used for further preparation of three LC sensors. Figure 4.6 shows the fabricated LC sensor 3 with dielectric paste on the capacitor part.

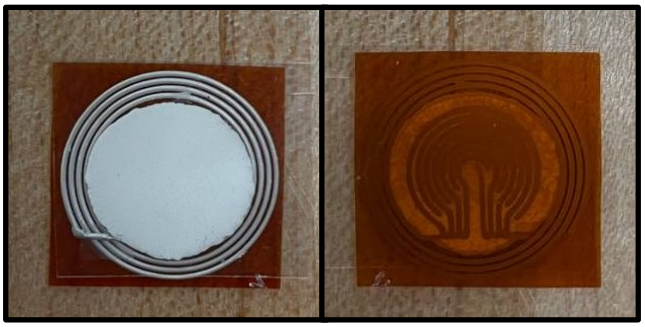

Figure 4.6. Actual image of LC sensor 3 with dielectric paste (40 wt. % of TiO_2) on top the capacitor.

Figure 4.7 shows the S21 measurement results for the working distance of 5 mm for three LC sensors without dielectric material and with dielectric paste on their capacitor. The blue line is for LC 1, the orange line is for LC 2, and the green line is for LC3. Solid lines are results from sensors without dielectrics, and dotted lines are results from sensors with dielectric paste. As shown in the graph, the resonant frequency of each LC sensor decreases by adding the dielectric material on top of its capacitor. By increasing the dielectric constant between the layers of a capacitor, the capacitance increases, so the resonant frequency decreases as expected based on equation 1.1.

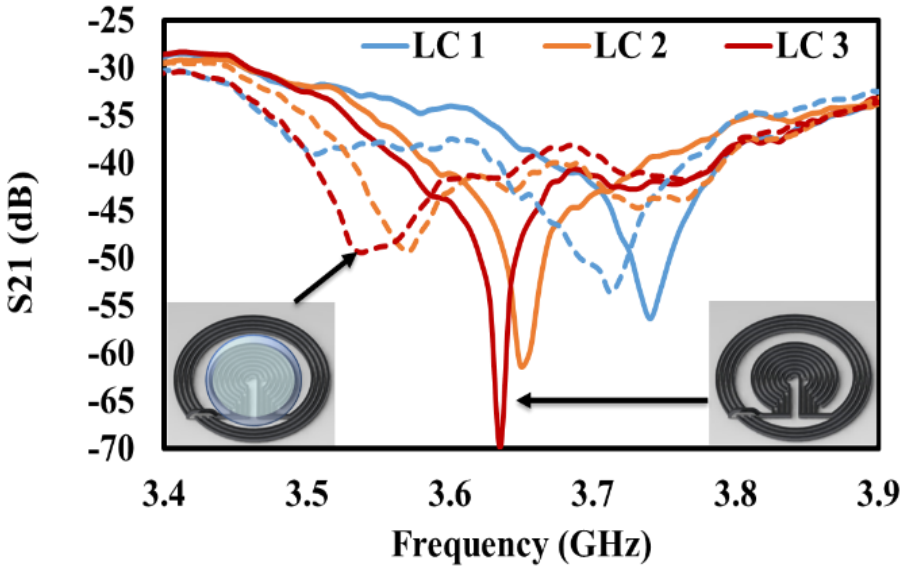

Figure 4.7. S21 measurement results for LC sensors with and without dielectric paste with 40 wt. % of TiO_2.

To find the effect of dielectric materials with high permittivity on wireless communication of the LC sensors, LC sensor 3 has been demonstrated with S21 wireless measurement for both with and without dielectric material in different detection distances as shown in figure 4.8. Orange points are data coming from the LC 3 without dielectric material and blue points are for the LC 3 with the dielectric material. For the LC sensor without dielectric material, the quality factor decreases from 18 to 0 as the working distance increases from 1 cm to 7 cm, which means that the resonant frequency could not be found at a working distance beyond 7 cm. The decreasing rate of the quality factor is 2.852/cm for this case. However, for the LC sensor with TiO_2 dielectric material, by increasing the working

distance, the quality factor decreased from 13.78 to 3.11 as the working distance increased from 1 cm to 10 cm, and the decreasing rate of the quality factor is 1.111/cm which means that by having the dielectric material with high dielectric constant, the wireless communication is more reliable for a relatively longer working distance because the dielectric material with high permittivity helps the electromagnetic communication of the LC sensor with the strip line. Although the quality factor decreased by increasing the capacitance after applying the dielectric material to the capacitor based on equation 1.2, the rate of decreasing the quality factor by increasing the working distance is twice less than the rate for LC sensors without dielectric material.

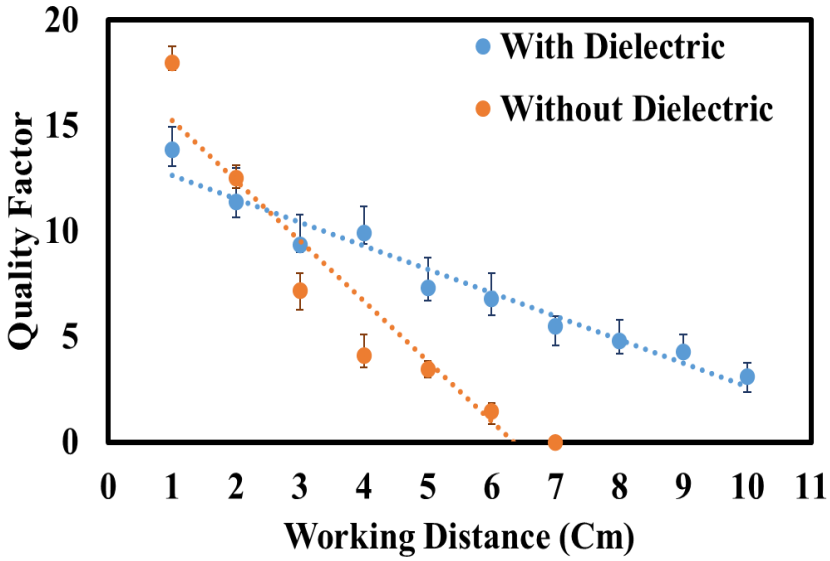

Figure 4.8. Quality factor of the LC sensor 3 with and without dielectric paste with 40 wt. % of TiO_2 in different working distances.

4.5. Conclusions

We demonstrated 3D printed LC sensors with monopole antenna for wireless identification of different locations. The S21 measurement of the reflection coefficient together with electro-magnetic FEA simulation has been conducted to verify measured resonant frequencies of LC sensors. It has been established that the designed LC sensors have distinctive resonant frequencies that can be employed for location-based sensing. Then, the transmission coefficient of the LC sensors on a strip-line antenna has been demonstrated. A wireless location identification utilizing the 3D-printed LC sensors has been demonstrated up to 10 cm working distance between the receiver antenna and sensors which has been increased 2.5 times in comparison with reported studies of LC sensors. Moreover, by applying a prepared high dielectric material on the capacitor part of the sensors which contains 40 wt. % TiO_2 that has a relative permittivity of 43, we demonstrate the enhanced wireless communication between the sensor tag and receiver.

Chapter 5. Conclusions and Future Work

5.1. Conclusions

Wireless communication offers opportunities for advances in the field of IoT and the connected world. Especially, by shifting towards robotics, wearable devices, and smart homes, wireless sensing technologies attracted lots of attention in the past few years. Several techniques and theories have been used for sensor designing in many applications which can affect the quality of human life and have needed to be improved and optimized in both design and fabrication to be successful in finding a place in daily life.

One sensing technology that has the greatest potential for taking the place of wireless sensing is RF-based sensors. They provide numerous merits such as wireless communication, reliable sensing mechanisms, easy operation, and in many cases working without the need for a power supply which is a great advantage in case of sustainability. Especially, LC wireless sensors are one of the famous groups of RF sensing. However, they have disadvantages such as short reading distance which limits their usage in many applications, and a relatively hard and time-consuming fabrication process of them.

Contrary to wireless LC sensors, chip-less RFID tag provides far-field wireless communication to the wireless reader, but mainly this technology has been used for identification application such as encoded key cards. By combining chip-less RFID tag technology and LC sensors, far-field wireless sensing in various applications can be potentially possible. In this research, we tried to propose a wireless sensing system consisting of RFID tag communication theory and LC sensors sensing abilities to achieve a reliable wireless sensor with far-field communication that can function in different applications by minimum alternation.

Moreover, conductive printing technologies provided several benefits for the fabrication of electronic devices and circuits. These fabrication processes are cost-effective in both time and materials, compatible with different systems such as sensor devices, and easy to control. Among these technologies, DIW 3D printing is one of the most advanced and suitable methods for printing circuits because it can print conductive complex patterns in

different layers with excellent mechanical properties without wasting any material. Here are three milestones in this thesis.

1. **Design and fabrication of 3D printed compact LC sensors**

   In this study, we designed three compact LC sensors suitable for DIW 3D printing. Each sensor has 3.75 turns of the inductor on the outside which is connected to the curved IDC at the center. The number of IDC fingers for three LC sensors is 4, 6, and 8 to have different resonant frequencies. After designing an RF tag with several parameters, both LC sensors and RF sensing tag have been fabricated by DIW 3D printing using conductive silver ink.

2. **FEA simulation of designed LC sensors**

   For the confirmation of compact LC sensor designs, the FEA simulation method has been used to confirm the performance of sensors. Results confirmed that three LC sensors have different resonant frequencies with distinct resonant frequencies. Moreover, the effects of using different dielectric materials for communication between LC sensors and RF tag have been studied by FEA simulation.

3. **Validation and demonstration of far-field RF sensors using a dielectric material with high dielectric constant**

   DIW 3D printed LC sensors and RF tag have been characterized with wireless RF testing. Results proved that the wireless communication between the reader and the printed RF sensor tag is possible up to 10 cm reading distance which has been improved by 250%, compared to other passive RF sensors. When the working distance is increased, the quality factor of the resonant frequency is decreased. Therefore, for better wireless communication, the printable TiO_2-based dielectric material with high electromagnetic permittivity has been prepared and printed on the LC sensors. The results confirmed that by using the dielectric paste, the quality of wireless communication has been improved, and by increasing the wireless reading distance, the quality factor decreases at a much lower rate. Table 3 summarizes the designed compact LC sensors and their resonant frequencies with and without TiO_2-based dielectric material.

Table 5.1 Three compact LC sensors and their resonant frequencies.

LC Sensor Number	Number of IDC Fingers	Resonant Frequency in RF tag Without TiO_2 Dielectric (GHz)	Resonant Frequency in RF tag With TiO_2 Dielectric Paste (GHz)
1	4	3.745	3.714
2	6	3.651	3.578
3	8	3.628	3.540

Overall, the work here describes the wireless sensing of proposed RF sensors for location identification. By achieving a chip-less, battery-less, far-field wireless sensor made by DIW 3D printing, it is demonstrated that this type of sensor system can be a strong candidate for wireless passive sensing applications such as robotics, wearable devices, or IoT. Achieving a far-field wireless sensing platform which can be utilized in various applications by minimum modification such as adding an extra parts or altering an existed part is the main contribution of this study.

5.2. Future Work

In this work, compact RF sensor tags were designed and fabricated. However, the focus of this research was on sensing performance for far-field wireless communications and using LC sensors as location identification on an RF tag. For the useful demonstration of the proposed wireless RF sensor tags in different applications, some modifications are required in the design of LC sensors. For instance, by modification of the capacitor part of the designed LC sensors, those sensors fit the pressure sensing applications. Therefore, future works can be dedicated to exploring the vast applications in other physical sensing areas. Future works can be dedicated to those applications such as pressure, temperature, or strain sensing by slight modification and tuning of the proposed compact RF sensors.

References

[1] M. Javaid, A. Haleem, R. P. Singh, S. Rab, and R. Suman, “Significance of sensors for industry 4.0: Roles, capabilities, and applications,” *Sensors International*, vol. 2, p. 100110, 2021.

[2] D. Sehrawat and N. S. Gill, “Smart sensors: Analysis of different types of IOT sensors,” *2019 3rd International Conference on Trends in Electronics and Informatics (ICOEI)*, 2019.

[3] F. Xu, X. Li, Y. Shi, L. Li, W. Wang, L. He, and R. Liu, “Recent developments for flexible pressure sensors: A Review,” *Micromachines*, vol. 9, no. 11, p. 580, 2018.

[4] M. Amjadi, K.-U. Kyung, I. Park, and M. Sitti, “Stretchable, skin-mountable, and wearable strain sensors and their potential applications: A Review,” *Advanced Functional Materials*, vol. 26, no. 11, pp. 1678–1698, 2016.

[5] B. Arman Kuzubasoglu and S. Kursun Bahadir, “Flexible temperature sensors: A Review,” *Sensors and Actuators A: Physical*, vol. 315, p. 112282, 2020.

[6] M. A. Mamun and M. R. Yuce, “Recent progress in nanomaterial enabled chemical sensors for wearable environmental monitoring applications,” *Advanced Functional Materials*, vol. 30, no. 51, p. 2005703, 2020.

[7] N. A. Malik, P. Sant, T. Ajmal, and M. Ur-Rehman, “Implantable antennas for bio-medical applications,” *IEEE Journal of Electromagnetics, RF and Microwaves in Medicine and Biology*, vol. 5, no. 1, pp. 84–96, 2021.

[8] Z. Luo, X. Hu, X. Tian, C. Luo, H. Xu, Q. Li, Q. Li, J. Zhang, F. Qiao, X. Wu, V. Borisenko, and J. Chu, “Structure-property relationships in graphene-based strain and pressure sensors for potential artificial intelligence applications,” *Sensors*, vol. 19, no. 5, p. 1250, 2019.

[9] L. Lubna, H. Hameed, S. Ansari, A. Zahid, A. Sharif, H. T. Abbas, F. Alqahtani, N. Mufti, S. Ullah, M. A. Imran, and Q. H. Abbasi, “Radio Frequency Sensing and its innovative applications in diverse sectors: A comprehensive study,” *Frontiers in Communications and Networks*, vol. 3, 2022.

[10] Z. Meng, Y. Liu, N. Gao, Z. Zhang, Z. Wu, and J. Gray, “Radio Frequency Identification and sensing: Integration of wireless powering, sensing, and communication for Iiot Innovations,” *IEEE Communications Magazine*, vol. 59, no. 3, pp. 38–44, 2021.

[11] K. Zhang, Z. Li, Z. Meng, W. Zhou, N. Gao, and Z. Zhang, “UHF-HF integrated RFID sensor: A novel information interface for industrial integration,” *IEEE Sensors Journal*, vol. 22, no. 15, pp. 15477–15487, 2022.

[12] H. Wen, C. Chen, S. Li, Y. Shi, H. Wang, W. Guo, and X. Liu, “Array integration and far-field detection of biocompatible wireless LC pressure sensors,” *Small Methods*, vol. 5, no. 3, p. 2001055, 2021.

[13] S. Deif and M. Daneshmand, “Multiresonant chipless RFID array system for coating defect detection and corrosion prediction,” *IEEE Transactions on Industrial Electronics*, vol. 67, no. 10, pp. 8868–8877, 2020.

[14] Q.-A. Huang, L. Dong, and L.-F. Wang, “LC passive wireless sensors toward a wireless sensing platform: Status, prospects, and challenges,” *Journal of Microelectromechanical Systems*, vol. 25, no. 5, pp. 822–841, 2016.

[15] I. Bhar and N. Mandal, “Design of a noncontact passive LC-based level sensor with a readout system,” *IEEE Transactions on Instrumentation and Measurement*, vol. 71, pp. 1–9, 2022.

[16] F. Lu, Y. Guo, Q. Tan, T. Wei, G. Wu, H. Wang, L. Zhang, X. Guo, and J. Xiong, “Highly sensitive reentrant cavity-microstrip patch antenna integrated wireless passive pressure sensor for high temperature applications,” *Sensors*, vol. 2017, pp. 1–10, 2017.

[17] L. Ma, R. Wu, A. Patil, S. Zhu, Z. Meng, H. Meng, C. Hou, Y. Zhang, Q. Liu, R. Yu, J. Wang, N. Lin, and X. Y. Liu, “Full-textile wireless flexible humidity sensor for human physiological monitoring,” *Advanced Functional Materials*, vol. 29, no. 43, p. 1904549, 2019.

[18] C. M. Boutry, L. Beker, Y. Kaizawa, C. Vassos, H. Tran, A. C. Hinckley, R. Pfattner, S. Niu, J. Li, J. Claverie, Z. Wang, J. Chang, P. M. Fox, and Z. Bao, “Biodegradable and flexible arterial-pulse sensor for the wireless monitoring of blood flow,” *Nature Biomedical Engineering*, vol. 3, no. 1, pp. 47–57, 2019.

[19] T. Kim, C. Bao, M. Hausmann, G. Siqueira, T. Zimmermann, and W. S. Kim, “3D printed disposable wireless ion sensors with biocompatible cellulose composites,” *Advanced Electronic Materials*, vol. 5, no. 2, p. 1800778, 2018.

[20] J. T. Simonen, M. M. Andringa, K. M. Grizzle, S. L. Wood, and D. P. Neikirk, “Wireless sensors for monitoring corrosion in reinforced concrete members,” *Smart Structures and Materials 2004: Sensors and Smart Structures Technologies for Civil, Mechanical, and Aerospace Systems*, 2004.

[21] D. Lu, Y. Yan, R. Avila, I. Kandela, I. Stepien, M. H. Seo, W. Bai, Q. Yang, C. Li, C. R. Haney, E. A. Waters, M. R. MacEwan, Y. Huang, W. Z. Ray, and J. A. Rogers, “Bioresorbable, wireless, passive sensors as temporary implants for monitoring regional body temperature,” *Advanced Healthcare Materials*, vol. 9, no. 16, p. 2000942, 2020.

[22] Z. Sun, H. Fang, B. Xu, L. Yang, H. Niu, H. Wang, D. Chen, Y. Liu, Z. Wang, Y. Wang, and Q. Guo, “Flexible wireless passive LC pressure sensor with design methodology and cost-effective preparation,” *Micromachines*, vol. 12, no. 8, p. 976, 2021.

[23] W.-J. Deng, L.-F. Wang, L. Dong, and Q.-A. Huang, “LC wireless sensitive pressure sensors with microstructured PDMS dielectric layers for wound monitoring,” *IEEE Sensors Journal*, vol. 18, no. 12, pp. 4886–4892, 2018.

[24] L. Dong, L.-F. Wang, and Q.-A. Huang, “A passive wireless adaptive repeater for enhancing the readout of lc passive wireless sensors,” *IEEE Microwave and Wireless Components Letters*, vol. 26, no. 7, pp. 543–545, 2016.

[25] O. Kanoun, A. Bouhamed, R. Ramalingame, J. R. Bautista-Quijano, D. Rajendran, and A. Al-Hamry, “Review on conductive polymer/CNTS nanocomposites based flexible and stretchable strain and pressure sensors,” *Sensors*, vol. 21, no. 2, p. 341, 2021.

[26] Q. Tan, Y. Ji, W. Lv, F. Wu, H. Dong, W. Zhang, and J. Xiong, “Signal readout of LC Pressure Sensor operated in multi-dimensional rotating environment with dual-inductance resonator,” *Sensors and Actuators A: Physical*, vol. 296, pp. 178–185, 2019.

[27] K. Finkenzeller, *RFID Handbook* 2nd Edition. John Wiley & Sons, Ltd., 2003.

[28] U. Kaiser and W. Steinhagen, “A low-power transponder IC for high-performance identification systems,” *IEEE Journal of Solid-State Circuits*, vol. 30, no. 3, pp. 306–310, 1995.

[29] V. Chawla and D. Ha, “An overview of passive RFID,” *IEEE Communications Magazine*, vol. 45, no. 9, pp. 11–17, 2007.

[30] A. A. A. Ibrahim, K. Nisar, Y. K. Hzou and I. Welc“, "Review and Analyzing RFID Technology Tags and Applicatio”s," *2019 IEEE 13th International Conference on Application of Information and Communication Technologies (AICT)*, pp. 1-4, 2019.

[31] S. Preradovic and N. C. Karmakar, *Introduction in: Multiresonator-based chipless RFID.* New York, NY: Springer, 2012.

[32] P. Kalansuriya, N. Karmakar, and E. Viterbo, “Signal Space Representation of chipless RFID tag frequency signatures,” *2011 IEEE Global Telecommunications Conference - GLOBECOM 2011*, 2011.

[33] N. Zavanelli and W.-H. Yeo, “Advances in screen printing of conductive nanomaterials for stretchable electronics,” ACS Omega, vol. 6, no. 14, pp. 9344–9351, 2021.

[34] D. Deganello, J. A. Cherry, D. T. Gethin, and T. C. Claypole, “Patterning of micro-scale conductive networks using reel-to-reel flexographic printing,” Thin Solid Films, vol. 518, no. 21, pp. 6113–6116, 2010.

[35] B. J. RAMSEY, P. S. EVANS, and D. HARRISON, “A novel circuit fabrication technique using offset lithography,” Journal of Electronics Manufacturing, vol. 07, no. 01, pp. 63–67, 1997.

[36] G. L. Goh, H. Zhang, T. H. Chong, and W. Y. Yeong, “3D printing of multilayered and Multimaterial Electronics: A Review,” Advanced Electronic Materials, vol. 7, no. 10, p. 2100445, 2021.

[37] R. M. Cardoso, D. M. H. Mendonça, W. P. Silva, M. N. T. Silva, E. Nossol, R. A. B. da Silva, E. M. Richter, and R. A. A. Muñoz, “3D printing for electroanalysis: From multiuse electrochemical cells to sensors,” Analytica Chimica Acta, vol. 1033, pp. 49–57, 2018.

[38] K. Kim, J. Park, J.-hoon Suh, M. Kim, Y. Jeong, and I. Park, “3D printing of multiaxial force sensors using carbon nanotube (cnt)/thermoplastic polyurethane (TPU) filaments,” Sensors and Actuators A: Physical, vol. 263, pp. 493–500, 2017.

[39] A. Kamyshny, “Metal-based inkjet inks for printed electronics,” The Open Applied Physics Journal, vol. 4, no. 1, pp. 19–36, 2011.

[40] F. Torrisi, T. Hasan, W. Wu, Z. Sun, A. Lombardo, T. S. Kulmala, G.-W. Hsieh, S. Jung, F. Bonaccorso, P. J. Paul, D. Chu, and A. C. Ferrari, “Inkjet-printed graphene electronics,” ACS Nano, vol. 6, no. 4, pp. 2992–3006, 2012.

[41] J. A. Lewis, “Direct ink writing of 3D functional materials,” *Advanced Functional Materials*, vol. 16, no. 17, pp. 2193–2204, 2006.

[42] D. V. Baker, C. Bao, and W. S. Kim, “Highly conductive 3D printable materials for 3D structural electronics,” *ACS Applied Electronic Materials*, vol. 3, no. 6, pp. 2423–2433, 2021.

[43] Y. Zhang, G. Shi, J. Qin, S. E. Lowe, S. Zhang, H. Zhao, and Y. L. Zhong, “Recent progress of direct ink writing of electronic components for Advanced Wearable Devices,” *ACS Applied Electronic Materials*, vol. 1, no. 9, pp. 1718–1734, 2019.

[44] T. Chu, S. Park, and K. (K. Fu, “3D printing-enabled Advanced Electrode Architecture Design,” Carbon Energy, vol. 3, no. 3, pp. 424–439, 2021.

[45] T. Kim, M. Kaur, and W. S. Kim, “Humanoid robot actuation through precise chemical sensing signals,” *Advanced Materials Technologies*, vol. 4, no. 11, p. 1900570, 2019.

[46] C. Bao, S. K. Seol, and W. S. Kim, “A 3D integrated neuromorphic chemical sensing system,” *Sensors and Actuators B: Chemical*, vol. 332, p. 129527, 2021.

[47] C. Bao, T.-H. Kim, A. Hassanpoor Kalhori, and W. S. Kim, “A 3D-printed neuromorphic humanoid hand for grasping unknown objects,” *iScience*, vol. 25, no. 4, p. 104119, 2022.

[48] H. Minemawari, T. Yamada, H. Matsui, J. Tsutsumi, S. Haas, R. Chiba, R. Kumai, and T. Hasegawa, “Inkjet printing of single-crystal films,” *Nature*, vol. 475, no. 7356, pp. 364–367, 2011.

[49] Y. Han and J. Dong, “Electrohydrodynamic (EHD) printing of molten metal ink for flexible and stretchable conductor with self-healing capability,” *Advanced Materials Technologies*, vol. 3, no. 3, p. 1700268, 2017.

[50] Z. Zhang, X. Zhang, Z. Xin, M. Deng, Y. Wen, and Y. Song, “Synthesis of monodisperse silver nanoparticles for ink-jet printed flexible electronics,” *Nanotechnology*, vol. 22, no. 42, p. 425601, 2011.

[51] T. Araki, T. Uemura, S. Yoshimoto, A. Takemoto, Y. Noda, S. Izumi, and T. Sekitani, “Wireless monitoring using a stretchable and transparent sensor sheet containing metal nanowires,” *Advanced Materials*, vol. 32, no. 15, p. 1902684, 2019.

[52] E. A. Ozek, S. Tanyeli, and M. K. Yapici, “Flexible graphene textile temperature sensing RFID coils based on spray printing,” *IEEE Sensors Journal*, vol. 21, no. 23, pp. 26382–26388, 2021.

[53] A. Vena, A. A. Babar, L. Sydanheimo, L. Ukkonen, and M. M. Tentzeris, “A novel wireless inkjet-printed chipless sensor for moisture detection utilizing carbon nanotube,” *2013 IEEE Antennas and Propagation Society International Symposium (APSURSI)*, 2013.

[54] I. J. Fernandes, A. F. Aroche, A. Schuck, P. Lamberty, C. R. Peter, W. Hasenkamp, and T. L. Rocha, “Silver nanoparticle conductive inks: Synthesis, characterization, and fabrication of inkjet-printed flexible electrodes,” *Scientific Reports*, vol. 10, no. 1, 2020.

[55] S. Hong, J. Yeo, G. Kim, D. Kim, H. Lee, J. Kwon, H. Lee, P. Lee, and S. H. Ko, “Nonvacuum, maskless fabrication of a flexible metal grid transparent conductor by low-temperature selective laser sintering of nanoparticle ink,” *ACS Nano*, vol. 7, no. 6, pp. 5024–5031, 2013.

[56] J. Perelaer, B.-J. de Gans, and U. S. Schubert, “Ink-jet printing and microwave sintering of Conductive Silver Tracks,” *Advanced Materials*, vol. 18, no. 16, pp. 2101–2104, 2006.

[57] K. Brinker and R. Zoughi, “Tunable chipless RFID pressure sensor utilizing additive manufacturing,” *2022 IEEE International Instrumentation and Measurement Technology Conference (I2MTC)*, 2022.

[58] B. Nie, R. Huang, T. Yao, Y. Zhang, Y. Miao, C. Liu, J. Liu, and X. Chen, “Textile-based Wireless Pressure Sensor Array for human-interactive sensing,” *Advanced Functional Materials*, vol. 29, no. 22, p. 1808786, 2019.

[59] H. Jeong, Y. Noh, S. H. Ko, and D. Lee, “Flexible resistive pressure sensor with silver nanowire networks embedded in polymer using natural formation of Air Gap,” *Composites Science and Technology*, vol. 174, pp. 50–57, 2019.

[60] J. Park, J.-K. Kim, S. Patil, J.-K. Park, S. A. Park, and D.-W. Lee, “A wireless pressure sensor integrated with a biodegradable polymer stent for biomedical applications,” *Sensors*, vol. 16, no. 6, p. 809, 2016.

[61] S. Khuje, A. Sheng, J. Yu, and S. Ren, “Flexible copper nanowire electronics for wireless dynamic pressure sensing,” *ACS Applied Electronic Materials*, vol. 3, no. 12, pp. 5468–5474, 2021.

[62] C. P. Yue and S. S. Wong, “On-chip spiral inductors with patterned ground shields for si-based RF ICS,” *IEEE Journal of Solid-State Circuits*, vol. 33, no. 5, pp. 743–752, 1998.

[63] Y. Zhai, J. Lee, Q. Hoang, D. Sievenpipper, H. Garudadri, and T. N. Ng, “A printed wireless fluidic pressure sensor,” *Flexible and Printed Electronics*, vol. 3, no. 3, p. 035006, 2018.

[64] T. Rai, P. Dantes, B. Bahreyni, and W. S. Kim, “A stretchable RF antenna with silver nanowires,” *IEEE Electron Device Letters*, vol. 34, no. 4, pp. 544–546, 2013.

[65] F. Nikbakhtnasrabadi, E. S. Hosseini, S. Dervin, D. Shakthivel, and R. Dahiya, “Smart bandage with inductor-capacitor resonant tank based printed wireless pressure sensor on Electrospun poly-l-lactide nanofibers,” *Advanced Electronic Materials*, vol. 8, no. 7, p. 2101348, 2022.

[66] M. G. Mohammed and R. Kramer, “All-printed flexible and Stretchable Electronics,” *Advanced Materials*, vol. 29, no. 19, p. 1604965, 2017.

[67] Y. Liu, M. Pharr, and G. A. Salvatore, “Lab-on-skin: A review of flexible and Stretchable Electronics for wearable health monitoring,” *ACS Nano*, vol. 11, no. 10, pp. 9614–9635, 2017.

[68] K. Qi, J. He, H. Wang, Y. Zhou, X. You, N. Nan, W. Shao, L. Wang, B. Ding, and S. Cui, “A highly stretchable nanofiber-based electronic skin with pressure-, strain-, and flexion-sensitive properties for health and motion monitoring,” *ACS Applied Materials & Interfaces*, vol. 9, no. 49, pp. 42951–42960, 2017.

[69] H. Jo, J.-W. Park, B. F. J. Spencer, and H.-J. Jung, “Development of high-sensitivity wireless strain sensor for Structural Health Monitoring,” *Smart Structures and Systems*, vol. 11, no. 5, pp. 477–496, 2013.

[70] R. Stoney, D. Geraghty, and G. E. O'Donnell, “Characterization of differentially measured strain using passive wireless surface acoustic wave (SAW) strain sensors,” *IEEE Sensors Journal*, vol. 14, no. 3, pp. 722–728, 2014.

[71] H. Jeong and S. Lim, “A stretchable radio-frequency strain sensor using screen printing technology,” *Sensors*, vol. 16, no. 11, p. 1839, 2016.

[72] L. Shu, B. Peng, Z. Yang, R. Wang, S. Deng, and X. Liu, “High-temperature saw wireless strain sensor with langasite,” *Sensors*, vol. 15, no. 11, pp. 28531–28542, 2015.

[73] J. Kim, Z. Wang, and W. S. Kim, “Stretchable RFID for wireless strain sensing with Silver Nano Ink,” *IEEE Sensors Journal*, vol. 14, no. 12, pp. 4395–4401, 2014.

[74] S.-H. Min, H.-J. Kim, Y.-J. Quan, H.-S. Kim, J.-H. Lyu, G.-Y. Lee, and S.-H. Ahn, “Stretchable chipless RFID multi-strain sensors using direct printing of aerosolised nanocomposite,” *Sensors and Actuators A: Physical*, vol. 313, p. 112224, 2020.

[75] G.-Y. Lee, J.-I. Park, C.-S. Kim, H.-S. Yoon, J. Yang, and S.-H. Ahn, “Aerodynamically focused nanoparticle (AFN) printing: Novel direct printing technique of solvent-free and inorganic nanoparticles,” *ACS Applied Materials & Interfaces*, vol. 6, no. 19, pp. 16466–16471, 2014.

[76] A. Salim, A. H. Naqvi, E. Park, A. D. Pham, and S. Lim, “Inkjet printed Kirigami inspired split ring resonator for disposable, low cost strain sensor applications,” *Smart Materials and Structures*, vol. 29, no. 1, p. 015016, 2019.

[77] P. Roriz, S. Silva, O. Frazão, and S. Novais, “Optical fiber temperature sensors and their biomedical applications,” *Sensors*, vol. 20, no. 7, p. 2113, 2020.

[78] H. Kairm, D. Delfin, M. A. Shuvo, L. A. Chavez, C. R. Garcia, J. H. Barton, S. M. Gaytan, M. A. Cadena, R. C. Rumpf, R. B. Wicker, Y. Lin, and A. Choudhuri, “Concept and model of a metamaterial-based passive wireless temperature sensor for harsh environment applications,” *IEEE Sensors Journal*, vol. 15, no. 3, pp. 1445–1452, 2015.

[79] T. Adiono, M. Y. Fathany, S. Fuada, I. G. Purwanda, and S. F. Anindya, “A portable node of humidity and temperature sensor for indoor environment monitoring,” *2018 3rd International Conference on Intelligent Green Building and Smart Grid (IGBSG)*, 2018.

[80] E. Sisinni, A. Depari, and A. Flammini, “Design and implementation of a wireless sensor network for temperature sensing in hostile environments,” *Sensors and Actuators A: Physical*, vol. 237, pp. 47–55, 2016.

[81] A. Vaz, A. Ubarretxena, I. Zalbide, D. Pardo, H. Solar, A. Garcia-Alonso, and R. Berenguer, “Full passive UHF tag with a temperature sensor suitable for human body temperature monitoring,” *IEEE Transactions on Circuits and Systems II: Express Briefs*, vol. 57, no. 2, pp. 95–99, 2010.

[82] Y. Shao, L. Wei, X. Wu, C. Jiang, Y. Yao, B. Peng, H. Chen, J. Huangfu, Y. Ying, C. J. Zhang, and J. Ping, “Room-temperature high-precision printing of flexible wireless electronics based on Mxene Inks,” *Nature Communications*, vol. 13, no. 1, 2022.

[83] B. Zazoum, A. Bachri, and J. Nayfeh, “Functional 2D MXENE INKS for wearable electronics,” *Materials*, vol. 14, no. 21, p. 6603, 2021.

[84] K. Pan, Y. Fan, T. Leng, J. Li, Z. Xin, J. Zhang, L. Hao, J. Gallop, K. S. Novoselov, and Z. Hu, “Sustainable production of highly conductive multilayer graphene ink for wireless connectivity and IOT Applications,” *Nature Communications*, vol. 9, no. 1, 2018.

[85] D. Girbau, A. Ramos, A. Lazaro, S. Rima, and R. Villarino, “Passive wireless temperature sensor based on time-coded UWB chipless RFID tags,” *IEEE*

Transactions on Microwave Theory and Techniques, vol. 60, no. 11, pp. 3623–3632, 2012.

[86] A. Albrecht, J. F. Salmeron, M. Becherer, P. Lugli, and A. Rivadeneyra, “Screen-printed chipless wireless temperature sensor,” *IEEE Sensors Journal*, vol. 19, no. 24, pp. 12011–12015, 2019.

[87] A. Macdonald, L. A. Hawkes, and D. K. Corrigan, “Recent advances in biomedical, Biosensor and clinical measurement devices for use in humans and the potential application of these technologies for the study of physiology and disease in wild animals,” *Philosophical Transactions of the Royal Society B: Biological Sciences*, vol. 376, no. 1831, p. 20200228, 2021.

[88] S. Ahmadzadeh, J. Luo, and R. Wiffen, “Review on biomedical sensors, Technologies and algorithms for diagnosis of sleep disordered breathing: Comprehensive survey,” *IEEE Reviews in Biomedical Engineering*, vol. 15, pp. 4–22, 2022.

[89] I. cheol Jeong, D. Bychkov, and P. C. Searson, “Wearable devices for precision medicine and Health State Monitoring,” *IEEE Transactions on Biomedical Engineering*, vol. 66, no. 5, pp. 1242–1258, 2019.

[90] E. Crowe, C. Scott, S. Cameron, J. H. Cundell, and J. Davis, “Developing wound moisture sensors: Opportunities and challenges for laser-induced graphene-based materials,” *Journal of Composites Science*, vol. 6, no. 6, p. 176, 2022.

[91] S. Amendola, C. Occhiuzzi, C. Miozzi, S. Nappi, F. Amato, F. Camera, and G. Marrocco, “UHF epidermal sensors: Technology and applications,” *Wearable Sensors*, pp. 133–161, 2021.

[92] V. Mazzaracchio, L. Fiore, S. Nappi, G. Marrocco, and F. Arduini, “Medium-distance affordable, flexible and wireless epidermal sensor for PH Monitoring in sweat,” *Talanta*, vol. 222, p. 121502, 2021.

[93] D. Okan, K. Woo, E. A. Ayello, and G. Sibbald, “The role of moisture balance in wound healing,” *Advances in Skin & Wound Care*, vol. 20, no. 1, pp. 39–53, 2007.

[94] S. Hasanpour, L. Karperien, T. Walsh, M. Jahanshahi, Z. Hadisi, K. J. Neale, B. R. Christie, N. Djilali, and M. Akbari, “A hybrid thread-based temperature and humidity sensor for continuous wound monitoring,” *Sensors and Actuators B: Chemical*, vol. 370, p. 132414, 2022.

[95] J. Salmerón, A. Albrecht, S. Kaffah, M. Becherer, P. Lugli, and A. Rivadeneyra, “Wireless chipless system for humidity sensing,” *Sensors*, vol. 18, no. 7, p. 2275, 2018.

[96] Y. Li, Z. Wei, and J. Huang, “An LC-type flexible wireless humidity sensor with electrospun isolation layer,” *2021 IEEE Sensors*, 2021.

[97] L. Corchia, G. Monti, E. D. Benedetto, and L. Tarricone, “A chipless humidity sensor for wearable applications,” *2019 IEEE International Conference on RFID Technology and Applications (RFID-TA)*, 2019.

[98] A. Beniwal, P. Ganguly, A. K. Aliyana, G. Khandelwal, and R. Dahiya, “Screen-printed graphene-carbon ink based disposable humidity sensor with wireless communication,” *Sensors and Actuators B: Chemical*, vol. 374, p. 132731, 2023.

[99] L. Marek, M. Campbell, M. Epton, M. Storer, and S. Kingham, “Real-time environmental sensors to improve health in the Sensing City,” *ISPRS - International Archives of the Photogrammetry, Remote Sensing and Spatial Information Sciences*, vol. XLI-B2, pp. 729–733, 2016.

[100] D. De Donno, L. Catarinucci, and L. Tarricone, “Ramses: RFID Augmented Module for Smart Environmental Sensing,” *IEEE Transactions on Instrumentation and Measurement*, vol. 63, no. 7, pp. 1701–1708, 2014.

[101] G. A. Eyebe and F. Domingue, “Towards substrate-sensitive chipless tags for sensing applications,” *2019 IEEE SENSORS*, 2019.

[102] A. A. Stekolshchikova, A. V. Radaev, O. Y. Orlova, K. G. Nikolaev, and E. V. Skorb, “Thin and flexible ion sensors based on Polyelectrolyte multilayers assembled onto the carbon adhesive tape,” *ACS Omega*, vol. 4, no. 13, pp. 15421–15427, 2019.

[103] A. Ivanova and K. Mikhelson, “Electrochemical properties of nitrate-selective electrodes: The dependence of resistance on the solution concentration,” *Sensors*, vol. 18, no. 7, p. 2062, 2018.

[104] T. Wu and S. Bhadra, “A printed LC resonator-based flexible RFID for remote potassium ion detection,” *IEEE Journal on Flexible Electronics*, vol. 1, no. 1, pp. 47–57, 2022.

[105] A. Vena, L. Sydanheimo, L. Ukkonen, and M. M. Tentzeris, “A fully inkjet-printed chipless RFID gas and temperature sensor on paper,” *2014 IEEE RFID Technology and Applications Conference (RFID-TA)*, 2014.

[106] A. T. Alreshaid, J. G. Hester, W. Su, Y. Fang, and M. M. Tentzeris, “Review—ink-jet printed wireless liquid and gas sensors for IOT, SmartAg and Smart City Applications,” *Journal of The Electrochemical Society*, vol. 165, no. 10, 2018.

[107] J. George, A. Abdelghani, P. Bahoumina, O. Tantot, D. Baillargeat, K. Frigui, S. Bila, H. Hallil, and C. Dejous, “CNT-based inkjet-printed RF gas sensor: Modification of substrate properties during the fabrication process,” *Sensors*, vol. 19, no. 8, p. 1768, 2019.

[108] R. Zhu, M. Desroches, B. Yoon, and T. M. Swager, “Wireless oxygen sensors enabled by Fe(II)-polymer wrapped carbon nanotubes,” *ACS Sensors*, vol. 2, no. 7, pp. 1044–1050, 2017.

[109] M. Hartwig, R. Zichner, and Y. Joseph, “Inkjet-printed wireless chemiresistive sensors—a review,” *Chemosensors*, vol. 6, no. 4, p. 66, 2018.

[110] K. Jha, A. Doshi, P. Patel, and M. Shah, “A comprehensive review on automation in agriculture using artificial intelligence,” *Artificial Intelligence in Agriculture*, vol. 2, pp. 1–12, 2019.

[111] J. M. Barcelo-Ordinas, J. Garcia-Vidal, M. Doudou, S. Rodrigo-Munoz, and A. Cerezo-Llavero, “Calibrating low-cost air quality sensors using multiple arrays of sensors,” *2018 IEEE Wireless Communications and Networking Conference (WCNC)*, 2018.

[112] W. M. Nooriman, A. H. Abdullah, N. A. Rahim, and K. Kamarudin, “Development of Wireless Sensor Network for Harumanis Mango Orchard's temperature, humidity and soil moisture monitoring,” *2018 IEEE Symposium on Computer Applications & Industrial Electronics (ISCAIE)*, 2018.

[113] Y. Feng, L. Xie, Q. Chen, and L.-R. Zheng, “Low-cost printed chipless RFID humidity sensor tag for intelligent packaging” *IEEE Sensors Journal*, vol. 15, no. 6, pp. 3201–3208, 2015.

[114] G. Stojanović, M. Radovanović, M. Malešev, and V. Radonjanin, “Monitoring of water content in building materials using a wireless passive sensor” *Sensors*, vol. 10, no. 5, pp. 4270–4280, 2010.

[115] E. Tan, W. Ng, R. Shao, B. Pereles, and K. Ong, “A wireless, passive sensor for quantifying packaged food quality” *Sensors*, vol. 7, no. 9, pp. 1747–1756, 2007.

[116] B. Nie, R. Huang, T. Yao, Y. Zhang, Y. Miao, C. Liu, J. Liu, and X. Chen, “Textile-based Wireless Pressure Sensor Array for human-interactive sensing” *Advanced Functional Materials*, vol. 29, no. 22, p. 1808786, 2019.

Appendix. Performance Control of Different RF Tag Designs

For designing the tag with specific parameters such as length and width of the strip line, and for finding the proper place for LC sensors on the tag, FEA simulation of effects of those parameters on resonant frequency for three designed sensors has been conducted and results have been provided in figure A.1. Based on the simulation results, the final design has been chosen to have biggest differences between resonant frequencies of three LC sensors.

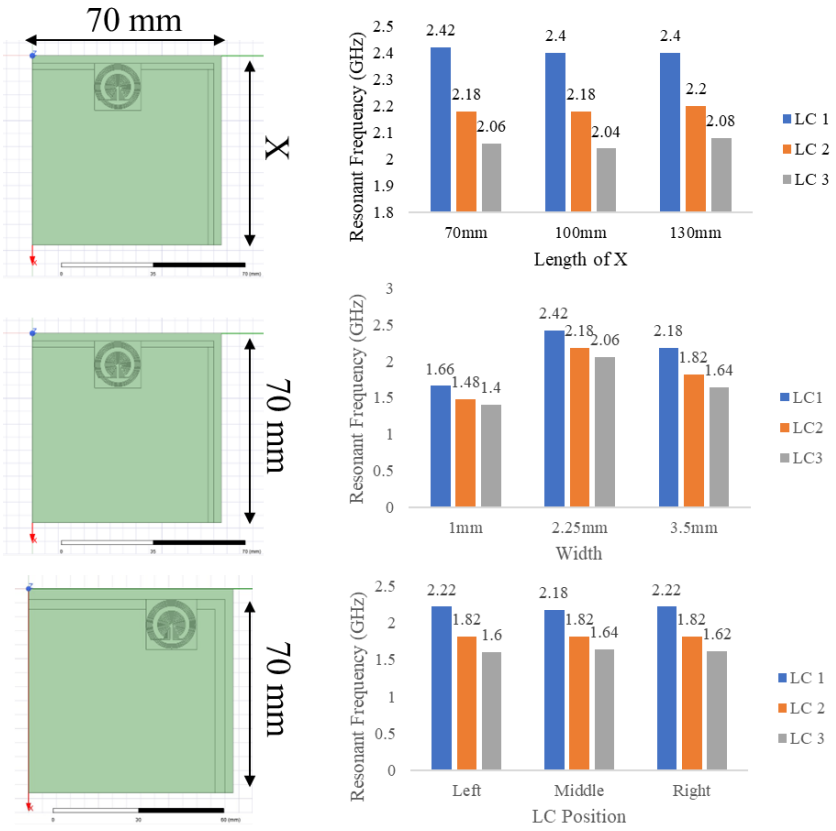

Figure A.1: FEA Simulation results of resonant frequency changes based on RF tag design.